

# DATA-ADAPTIVE ESTIMATION OF TIME-VARYING SPECTRAL DENSITIES

ANNE VAN DELFT AND MICHAEL EICHLER

*Maastricht University*

January 1, 2024

**ABSTRACT.** This paper introduces a data-adaptive approach for spectral density estimation of nonstationary processes. Estimation of time-dependent spectra commonly proceeds by means of local kernel smoothing. The performance of these nonparametric estimators depends however crucially on the smoothing bandwidths that need to be specified in both time and frequency direction. The objective of this paper is to construct local spectral density estimates where the respective smoothing kernels are iteratively adapted to the data at hand. The main idea, inspired by the concept of propagation-separation (Polzehl and Spokoiny 2006), is to describe the largest local vicinity of every design point in the time-frequency plane over which smoothing is justified by the data. Our method circumvents the problem of optimal bandwidth selection in the strict sense without imposing additional assumptions. The procedure permits full flexibility for the degree of smoothing and automatically adjusts for structural breaks in the time-dependent spectrum.

*Keywords:* Local stationary processes, time-varying spectral density, data-adaptive kernel estimation

*2010 Mathematics Subject Classification.* Primary: 62M10; Secondary: 62M15.

## 1. INTRODUCTION

Spectral analysis of time series data has been of interest for many years and has a varied history owing to applications in a wide range of disciplines such as geophysics, astronomy, sound analysis, analysis of medical data or yet of economical data. There exists a rather extensive literature on spectral analysis of weakly stationary processes and statistical techniques are well developed (Cramér 1942, Bartlett 1950, Grenander and Rosenblatt 1957, Cooley and Tukey 1965, Brillinger 1981). However, in most aforementioned applications the time series show nonstationary behavior and imposing weak stationarity is too restrictive. Especially when data is measured over longer periods of time, it is more plausible that the dynamics of the process change thereby invalidating the stationarity assumption. For this reason, the analysis of nonstationary time series has received more attention over the years.

Despite of its importance, the extension of existing estimation methods to processes that are not generated by time-invariant mechanisms is not a natural one. Classical asymptotic theory is by definition conflicting with the idea that the underlying probabilistic structure of the process changes over time. Two main approaches that deal with time-varying spectra are provided in the literature. In one approach, it is assumed that signals are subject to structural breaks and can be considered

piecewise stationary. For example, Ombao et al. (2001) introduce a method to automatically split the signal into piecewise stationarity segments and select the span of SLEX (Smooth Localised Complex Exponentials) basis functions used to obtain smoothed estimates of the time-varying spectrum. Another approach, which was first considered by Priestley (1965), is to assume the underlying dynamics change slowly such that a smooth time-dependent spectrum exists and, at a local level, the process is approximately stationary. The locally stationary setting of Dahlhaus (1996b) provides a framework for meaningful inference of these type of processes and comprises weak stationarity as a special case. We will adopt the latter theoretical framework as to include applications that exhibit slowly changing behavior. At the same time our procedure will automatically adjust to possible structural breaks in the spectrum.

A well-known difficulty for inference on the latter type of processes is the necessity of local estimates of the time-dependent spectrum which requires kernel smoothing at a local level. As for nonparametric estimation in general, inherent to these methods is the issue of bandwidth selection. Although this problem also arises in the stationary case where a bandwidth in frequency direction needs to be set, the time-varying case requires additionally specification of a bandwidth in time direction. Time-dependent spectral density estimation becomes therefore a two-dimensional problem in which one needs to be able to adjust for possible different degrees of smoothness of the spectrum in both directions. Proper adjustment is important in practice since the accuracy of corresponding estimates has been shown to be quite sensitive to the choice of smoothing bandwidths in both time as well as frequency direction. See for example Eichler et al. (2011), who investigate principal component analysis in the frequency domain for time-varying dynamic factor models. Theoretical optimal bandwidths depend on the unknown underlying spectrum and no guidelines are available on how to set them in practice (Dahlhaus 2009). To our knowledge, data-adaptive schemes have not yet been considered. Under specific parametric assumptions there are however methods available based on the segmented periodogram. For example, Sergides and Paparoditis (2009) and Preuß et al. (2011) use an integrated version to test for semi-parametric hypotheses which avoids bandwidth selection in frequency direction. The major drawback of such underlying estimate is that a fixed time bandwidth must be set which complicates, for example, detecting a possible break in the spectrum.

The objective of this paper is to construct local spectral density estimates where the respective smoothing kernels are adapted to the data at hand. This approach circumvents the problem of optimal bandwidth selection in the strict sense and permits full flexibility for the degree of smoothing. The procedure is based on the propagation-separation approach introduced by Polzehl and Spokoiny (2006) who investigate local likelihood estimation of exponential family models. The general idea behind it is to determine a maximal local neighborhood of a design point  $f_i$  such that some local parametric assumption is still justified by the data. One starts with a small local neighborhood to estimate the parameter value and, during each step, the neighborhood is extended to include new data points for which the parametric assumption is not violated. This property is referred to as propagation. At the same time, points for which the assumption is violated are not included, i.e., areas will be separated in that case.

We introduce a bivariate propagation–separation approach to estimate the structure of the time–dependent spectrum of nonstationary time series over the time–frequency plane  $U \times \Pi := [0, 1] \times [-\pi \times \pi]$ . For each design point in the plane, a maximal local neighborhood is determined iteratively over which smoothing is justified by the data. More specifically, the neighborhood used for estimation in step  $k$  of a local spectral variate  $f(u_l, \lambda_i)$  will be described by a set of weights  $\{W_{l,i}^{(k)}(s, j)\}$  that defines the shape of the kernel and is derived using the spectral estimates constructed at the previous step,  $k - 1$ . The effective neighborhood over which is smoothed for estimation in step  $k$  is then given by the points for which the corresponding weights from step  $k - 1$  are significantly different from zero. The big advantage is that the various design points are allowed to have kernels that are constructed with different weights functions leading to full adjustability in terms of shape and effective bandwidths. This is especially important in the presence of peaks or breaks for which a smaller effective bandwidth will reduce the problem of over–smoothing. At the same time, we will be able to get more accuracy in stable areas as the effective bandwidth is permitted to be relatively larger than would a global bandwidth have been set. It is worth remarking that the smoothing kernels can in fact be asymmetric. In particular, this feature of the method enables automatic adjustment to the presence of breaks in the spectrum. It should moreover be pointed out that the extension to the frequency domain is not obvious as the assumptions underlying the case of Polzehl and Spokoiny (2006) do not hold nor do we apply the principle of propagation–separation in the same manner.

Our paper is organized as follows. In section 2, we describe the type of processes of interest and introduce the building blocks of the estimator. Then, in section 3, the procedure is discussed while section 4 describes the effect of the choice of parameters and general guidelines are given. In section 5, the properties of the approach are illustrated by application to simulated data. In section 6, the approach is applied to Local Field Potential recordings.

## 2. THEORETICAL FRAMEWORK: LOCALLY STATIONARY PROCESSES

Before we introduce the procedure, we first discuss what we mean by time-dependent spectra and how they can be estimated. Since there is no time–dependent spectrum that is linearly connected to the covariance function of the process and at the same time keeps all nice underlying properties that exist in the weakly stationary case, different definitions for time-dependent spectra have been provided in the literature (e.g. Priestley 1965, Subba Rao 1970, Martin 1985, Hallin 1986). Most definitions depend in the classical way on  $T$ , the length of the time series, and therefore do not provide a meaningful asymptotic framework as future observations will generally not provide any relevant information of the probabilistic structure over the observed time period. In order to exploit large-sample properties at a local level, we shall adhere to the theoretical framework of locally stationary processes as introduced by Dahlhaus (1996b) which is based on infill asymptotics. Instead of considering the same process for larger values of  $T$ , the idea of this approach is to redefine the process in such a way that one observes the parameter curves on a finer grid so that a more and more dense design is obtained as  $T$  tends to infinity. For example, for a time-varying autoregressive process of order 1, this leads to a sequence of processes

$\{X_{t,T}\}$ 

$$X_{t,T} = a\left(\frac{t}{T}\right)X_{t-1,T} + \sigma\left(\frac{t}{T}\right)\varepsilon_t, \quad t = 1, \dots, T, T \in \mathbb{N}, \quad (2.1)$$

where  $a(\cdot)$  and  $\sigma(\cdot)$  are real-valued continuous functions on  $[0, 1]$ . The time-varying parameters of  $X_{t,T}$  depend then also on  $T$  such that for increasing  $T$  one obtains more and more observations with approximately the same dynamic dependence. Thus such families of processes provide a framework for asymptotic analysis permitting the researcher to consider properties of estimators such as consistency or asymptotic normality. We emphasize that this framework is purely theoretical as in practice  $T$  is fixed and increasing  $T$  will lead to considering a different time series. Put differently, if we increase  $T$ , we consider a different ‘level’ in the family than that we have data for. This discrepancy should be kept in mind when applying asymptotic results in practice to approximate those for finite  $T$ . Processes that can be analyzed by this framework must be locally approximately stationary in the sense that over short time periods they can be well approximated by a stationary process while their characteristics such as the covariance structure and parameters change gradually over longer time periods. More specifically, we assume (Dahlhaus 1996b):

**Definition 2.1 (Local stationarity).** A sequence of stochastic processes  $\{X_{t,T}, t = 1, \dots, T, T \in \mathbb{N}\}$  is called locally stationary with transfer function  $A^\circ$  and mean function  $\mu$  if there exists a representation

$$X_{t,T} = \mu\left(\frac{t}{T}\right) + \int_{-\pi}^{\pi} e^{i\lambda t} A_{t,T}^\circ(\lambda) d\xi(\lambda) \quad (2.2)$$

with the following properties:

- (i)  $\xi(\lambda)$  is a stochastic increment process defined on  $[-\pi, \pi]$  with  $\overline{\xi(\lambda)} = \xi(-\lambda)$ ,  $\mathbb{E}(\xi_a(\lambda)) = 0$  such that

$$\text{cum}(d\xi(\lambda_1), \dots, d\xi(\lambda_k)) = \eta\left(\sum_{j=1}^k \lambda_j\right) h_k(\lambda_1, \dots, \lambda_{k-1}) d\lambda_1, \dots, d\lambda_k,$$

where  $\text{cum}(\cdot)$  denotes the  $k$ -th order cumulant,  $h_k$  are cumulant densities with  $h_1 = 0$ ,  $h_2(\lambda) = 1$ , and  $|h_k(\lambda_1, \dots, \lambda_{k-1})| \leq C_k$  for all  $k \in \mathbb{N}$ , and  $\eta(\lambda) = \sum_{j \in \mathbb{Z}} \delta(\lambda + 2\pi j)$  is the  $2\pi$ -periodic extension of the Dirac delta function.

- (ii) There exist a constant  $C$  and a  $2\pi$ -periodic smooth function  $A : [0, 1] \times \mathbb{R} \rightarrow \mathbb{C}$  with  $\overline{A(u, \lambda)} = A(u, -\lambda)$  such that

$$\sup_{t, \lambda} \left| A_{t,T}^\circ(\lambda) - A\left(\frac{t}{T}, \lambda\right) \right| \leq \frac{C}{T} \quad (2.3)$$

for all  $T \in \mathbb{N}$ .

With this spectral representation, the time-varying spectral density of the process  $\{X_{t,T}\}$  is defined as

$$f(u, \lambda) = \frac{1}{2\pi} A(u, \lambda) A(u, \lambda)^* \quad (2.4)$$

for  $u \in [0, 1]$  and  $\lambda \in [-\pi, \pi]$ . If the transfer function  $A(u, \lambda)$  is smooth,  $f(u, \lambda)$  is the mean square limit of the Wigner–Ville spectrum (Martin 1985)

$$f_T(u, \lambda) = \frac{1}{2\pi} \sum_{s=-\infty}^{\infty} \text{cov}(X_{[uT-s/2],T}, X_{[uT+s/2],T}) e^{-is\lambda}, \quad (2.5)$$

where the processes  $X_{t,T}$  are extended on  $\mathbb{Z}$  by setting  $A_{t,T}^\circ(\lambda) = A_{1,T}^\circ(\lambda)$  for  $t < 1$  and  $A_{t,T}^\circ(\lambda) = A_{T,T}^\circ(\lambda)$  for  $t > T$ . As explained in Dahlhaus (1996b), the necessity of defining both  $A_{t,T}^\circ(\lambda)$  and  $A(u, \lambda)$  comes from the fact that for certain processes the spectral representation in (2.2) holds but the representation with a smooth common filter in continuous time for all  $T$  only holds approximately. The smoothness of the latter is however necessary to derive distributional properties. An important consequence of this approach, and something that is not possible in non-rescaled time for time-varying processes, is the uniqueness of the time-varying spectral density.

Since our interest lies in estimation of smooth time-varying spectral densities with possible breaks in the spectrum, we moreover assume the following condition holds:

**Assumption 2.2.**  *$\{X_{t,T}, t = 1, \dots, T, T \in \mathbb{N}\}$  is defined as in definition 2.1 and has spectral density  $f(u, \lambda)$  that is twice differentiable in  $\lambda$  and piecewise twice differentiable in  $u$  with bounded derivatives in both directions.*

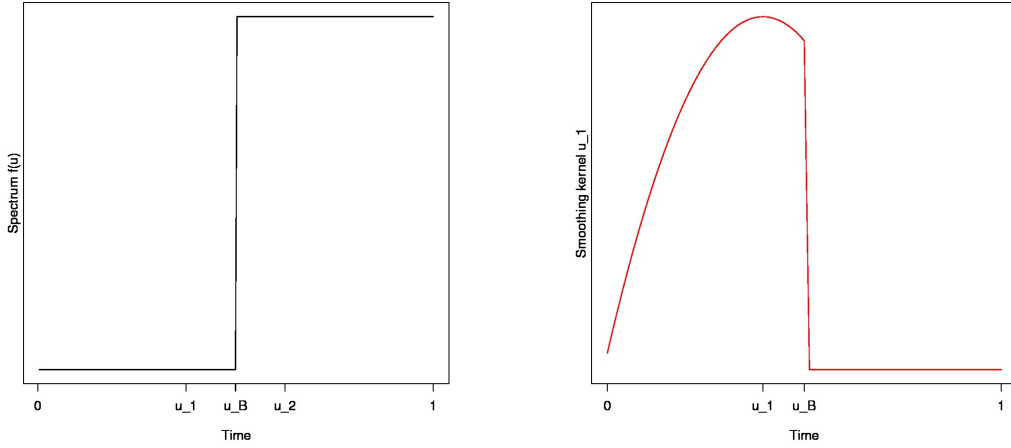
Throughout this paper, rescaled time on the unit interval  $\frac{t}{T}$  will be denoted by  $u$ . Furthermore, for sake of simplicity we assume that the mean function  $\mu$  is zero.

### 3. PROPAGATION-SEPARATION APPROACH IN THE TIME-FREQUENCY PLANE

Obtaining consistent estimates of the local time-varying spectrum requires smoothing in both time and frequency direction of some underlying raw estimator. Although various asymptotic results are available (see e.g. Dahlhaus 2009, Dahlhaus and Polonik 2009), determining the corresponding optimal smoothing bandwidths in practice is still an open problem. The purpose of this paper is to data-adaptively determine the shape of the smoothing kernels, which are then consequently used to obtain estimates of the local spectral variates. We start with small fixed bandwidths to obtain initial estimates. Then, at each iteration, the neighborhood used for estimation is extended in the direction for which the assumption of ‘homogeneity’ is still satisfied. We stop smoothing in those directions where it gets violated. This is achieved by means of a penalty kernel that penalizes regions not considered homogeneous.

#### 3.1. Motivating Example

To capture the main idea, imagine the simple case where we have a white noise signal with a break in time-direction at point  $u_b$  as given in Figure 3.1 (a). It should be clear that for point  $u_1$ , we do not want to smooth over point  $u_2$ , which lies on the other side of the break. On the other hand, we would like to smooth over as many data points on the left side of the break for the construction of the kernel of point  $u_1$  as the process is clearly stationary there. Ideally, the kernel should thus be constructed in such a way that it smooths as much as possible over the points on the left of the break but that gets cut off once we hit the break point. Our method allows for this by, in each iteration, comparing the data points in the extended neighborhood with each other in the so-called penalty step. Further smoothing only occurs if the data points are considered ‘similar’ by this step. For point  $u_1$ , we should therefore obtain a kernel as given in Figure 3.1 (b).



(a) Flat spectrum with break

(b) Ideal smoothing kernel at  $u_1$ 

FIGURE 3.1

A simplified version of the algorithm is as follows:

1. **Initialisation:** Construct initial estimates  $\hat{f}_T^{\text{in}}(u, \lambda)$  for all points in the time-frequency plane using small initial bandwidths  $b_{t,T}^{(0)}$  and  $b_{f,T}^{(0)}$  in time- and frequency direction, respectively.
2. **Penalty step:** For each point, compare the estimate with all other estimates in the initial smoothing neighborhood. If a point in this neighborhood is deemed ‘too different’, then that particular point receives less relative weight in construction of the adaptive kernel for the point of interest.
3. **Memory step:** Control for too fast changes and cross-interference terms by comparing the current with the previous estimate. Set  $k = 1$ .
4. **Increase searching bandwidth** to  $b_{t,T}^{(k)}, b_{f,T}^{(k)}$  and repeat penalty and memory step on the new estimates. Set  $k = k + 1$  and repeat until  $k = k_{\max}$ .

Before we discuss the algorithm in more detail, it should be clear that we need a couple of elements. Firstly, we require an underlying raw estimator to construct initial estimates. Secondly, we need to construct the adaptive estimator which is based on the penalty step. To allow for gradual changes in the spectrum and overall stability, we additionally need a memory step. We shall discuss these in turn.

### 3.2. A local estimator: the modified pre-periodogram

As an underlying raw estimator, most of the literature considers a segmented periodogram formed as a weighted average of fixed possibly overlapping time segments (e.g. Dahlhaus 1996b, Preuß et al. 2011). The optimal segment length, which should be set explicitly, is directly depending on the relation of smoothness in time- and frequency direction; a higher time resolution requires a shorter segment length but will yield a lower frequency resolution and vice versa. Another possibility is to use the pre-periodogram which is a localized version of the periodogram and was first introduced by Neumann and von Sachs (1997) who considered it for estimation of time-varying spectral densities by means of wavelets. Just like for the periodogram, the uncertainty principle still implies that the accuracy of estimation is limited by

the reciprocal relationship that exists between time and frequency resolution. The advantage of the pre-periodogram over the periodogram is however that the degree of smoothing in both time- and frequency direction is left to the smoothing step and therefore gives more freedom in adjusting for either direction based on local behavior of the observed process. Especially in our case, this is useful as we would like to adjust the kernel adaptively. For this reason, we shall use the pre-periodogram as underlying raw estimator. It is given by

$$J_T(u, \lambda) = \frac{1}{2\pi} \sum_{k: 1 \leq \lfloor uT + \frac{k+1}{2} \rfloor, T \leq \lfloor uT - \frac{k-1}{2} \rfloor, T} X_{\lfloor uT + \frac{k+1}{2} \rfloor, T} X_{\lfloor uT - \frac{k-1}{2} \rfloor, T} e^{-ik\lambda}. \quad (3.1)$$

Here, the term  $X_{\lfloor uT + \frac{k+1}{2} \rfloor, T} X_{\lfloor uT - \frac{k-1}{2} \rfloor, T}$  can be regarded as a preliminary estimator of the time-varying covariance function at rescaled time  $u$  and lag  $k$ , which is defined as the inverse Fourier transform of the time-varying spectral density,

$$\gamma(u, k) = \int_{-\pi}^{\pi} f(u, \lambda) e^{i\lambda k} d\lambda. \quad (3.2)$$

The ordinary periodogram can be recovered by averaging the pre-periodogram variates over  $t = 1, \dots, T$ . Its expectation for fixed  $T$  is moreover easily seen to coincide with the Wigner-Ville spectrum (2.5). If averaging is not done over all data points  $t$ , these type of preliminary estimators (Martin 1985) will suffer from the presence of cross-interference terms. This leads to bad behavior such as possible negative estimates. We tailored our method to be able to cope with this. As a first step, we use a slightly modified definition of the pre-periodogram as a preliminary estimator. For odd lags, the classical pre-periodogram shows an asymmetry about the central point  $t = uT$ . Cross-interference terms can be dampened by using an alternative symmetric definition that would place the product exactly at the midpoint  $\frac{t+s}{2}$ . For  $k = |t - s|$  odd, this is however not in line with one of the observations. We can take care of this by letting the preliminary covariance estimator average two neighboring covariances (in time) if no exact estimator is available. The idea is therefore to define the preliminary covariance estimator by

$$C^*(t, k) = \begin{cases} X_{t-\frac{k}{2}} X_{t+\frac{k}{2}} & \text{if } t \pm \frac{k}{2} \in \mathbb{Z}, \\ \frac{1}{2} (X_{t-\frac{k-1}{2}} X_{t+\frac{k-1}{2}} + X_{t+\frac{k+1}{2}} X_{t+\frac{k+1}{2}}) & \text{otherwise} \end{cases} \quad (3.3)$$

at time points  $t$  such that  $t \in \{1, \frac{3}{2}, 2, \frac{5}{2}, \dots, T-1, T-\frac{1}{2}, T\}$  and  $0 \leq u \leq \min\{2(t-1)/T, 2(T-1)/T\}$ . Outside the specified range, the estimator is set to zero. With this definition, the pre-periodogram now becomes

$$J_T(u, \lambda) = \frac{1}{2\pi} \sum_{k=-(T-1)}^{T-1} C^*(t, k) e^{-ik\lambda} \quad (3.4)$$

for time points  $u \in \{\frac{2}{2T}, \frac{3}{2T}, \dots, 1\}$ .

The pre-periodogram is asymptotically unbiased for the time-varying spectrum  $f(u, \lambda)$ . However, it is not consistent as its variance asymptotically diverges to infinity. A consistent estimator can be obtained by convolving the pre-periodogram

with kernel functions in both directions, i.e.,

$$\hat{f}_T(u, \lambda) = \frac{1}{b_{f,T} b_{t,T}} \int_0^1 \int_{-\pi}^{\pi} K_f\left(\frac{\lambda - \mu}{b_{f,T}}\right) K_t\left(\frac{u - v}{b_{t,T}}\right) J_T(v, \mu) d\mu dv, \quad (3.5)$$

where  $K_f$  and  $K_t$  denote the kernels for smoothing in frequency- and in time direction, respectively, and  $b_{f,T}$  and  $b_{t,T}$  are the corresponding bandwidths. The bandwidths should tend to zero at an appropriate rate as  $T \rightarrow \infty$ . In practice, smoothing of the pre-periodogram is based on a discretized version of the above kernel estimator

$$\hat{f}_T(u, \lambda) = \frac{1}{C} \sum_{s,j} K_f\left(\frac{\lambda - \lambda_j}{b_{f,T}}\right) K_t\left(\frac{u - s/T}{b_{t,T}}\right) J_T\left(\frac{s}{T}, \lambda_j\right), \quad (3.6)$$

where  $\lambda_j = \frac{\pi j}{T}$  for  $j = 1 - T, \dots, T$  denote the Fourier frequencies and  $C = \sum_{s,j} K_f((\lambda - \lambda_j)/b_{f,T}) K_t((u - s/T)/b_{t,T})$  is the normalization constant. The properties of (3.6) have been investigated in the setting of empirical spectral processes in Dahlhaus (2009) and Dahlhaus and Polonik (2009). In particular, it has been shown that under suitable conditions on the smoothness of the time-varying filter, the estimator is asymptotically normal (Theorem 3.2, Example 4.1 of Dahlhaus 2009). We use this estimator in the initialization step of the procedure.

### 3.3. Adaptive estimation of the time-dependent spectrum

In order to data-adaptively smooth the pre-periodogram, we consider a sequence of weighted averages

$$\hat{f}_T^{(k)}(u, \lambda) = \frac{1}{N_{u,\lambda}^{(k,T)}} \sum_{s,j} W_{u,\lambda}^{(k,T)}(s, j) J_T\left(\frac{s}{T}, \lambda_j\right) \quad k = 1, \dots, k_{max} \quad (3.7)$$

where  $J_T$  is the pre-periodogram given in (3.4) and  $N_{u,\lambda}^{(k,T)} = \sum_{s,j} W_{u,\lambda}^{(k,T)}(s, j)$  is the sum of weights. These weight sequences will thus determine the shape of the kernels of all points in the time-frequency plane. In each iteration  $k$ , we first construct in the penalty step an auxiliary kernel estimator

$$\tilde{f}_T^{(k)}(u, \lambda) = \frac{1}{\tilde{N}_{u,\lambda}^{(k,T)}} \sum_{s,j} \tilde{W}_{u,\lambda}^{(k,T)}(s, j) J_T\left(\frac{s}{T}, \lambda_j\right), \quad (3.8)$$

where the adaptive kernel weights  $\tilde{W}_{u,\lambda}^{(k,T)}$  depend not only on the distance between  $(u, \lambda)$  and  $(\frac{s}{T}, \lambda_j)$  but also on the difference between  $\hat{f}_T^{(k-1)}(u, \lambda)$  and  $\hat{f}_T^{(k-1)}(\frac{s}{T}, \lambda_j)$ , the estimates constructed in the previous iteration. More precisely, for fixed  $(u, \lambda)$ , the weights  $\tilde{W}_{u,\lambda}^{(k,T)}$  are given by

$$\tilde{W}_{u,\lambda}^{(k,T)}(s, j) = K_f\left(\frac{\lambda - \lambda_j}{\tilde{b}_{f,T,u,\lambda}^{(k)}}\right) K_t\left(\frac{u - s/T}{\tilde{b}_{t,T,u,\lambda}^{(k)}}\right) K_p\left(P^{(k,T)}[(u, \lambda), (\frac{s}{T}, \lambda_j)]\right) \quad (3.9)$$

and  $\tilde{N}_{u,\lambda}^{(k,T)} = \sum_{s,j} \tilde{W}_{u,\lambda}^{(k,T)}(s, j)$ . The bandwidths  $\tilde{b}_{t,T,u,\lambda}^{(k)}$  and  $\tilde{b}_{f,T,u,\lambda}^{(k)}$  of the localization kernels increase in  $k$  to allow a larger degree of smoothing in each iteration. These bandwidths can differ over the plane and are based on the previous effective bandwidth. That is,

$$\tilde{b}_{t,T,u,\lambda}^{(k)} = b_{T,u,\lambda}^{(k-1)} \gamma_t, \text{ and } \tilde{b}_{f,T,u,\lambda}^{(k)} = 2\pi b_{T,u,\lambda}^{(k-1)} \gamma_f, \quad (3.10)$$



where  $\gamma_t$  and  $\gamma_f$  are the growth rates in time- and frequency direction, respectively. Without loss of generality, the effective bandwidth is measured by  $(b_{T,u,\lambda}^{(k)})^2 = N_{u,\lambda}^{(k,T)}/T^2$ . To prevent over-smoothing, a penalty statistic  $P^{(k,T)}[(u, \lambda), (\frac{s}{T}, \lambda_j)]$  is used to compare the two local estimates  $\hat{f}_T^{(k-1)}(u, \lambda)$  and  $\hat{f}_T^{(k-1)}(\frac{s}{T}, \lambda_j)$  from the previous iteration, and any deviation in value is penalized by means of the penalty kernel  $K_p$ . Thus the resulting kernel assigns less weight to pre-periodogram variates that do not belong—based on the estimates from the previous step—to the local area of homogeneity about the point  $(u, \lambda)$ . We note that due to this construction the adaptive kernel in principle can be of *any shape*. If no penalization occurs, we obtain the usual kernel estimator in (3.6). Throughout the rest of the paper, the latter estimator will be referred to as the *nonadaptive estimator*.

The estimator at step  $k$ ,  $\hat{f}_T^{(k)}(u, \lambda)$ , is obtained by shifting the auxiliary estimator  $\tilde{f}_T^{(k)}(u, \lambda)$  towards the estimator  $\hat{f}_T^{(k-1)}(u, \lambda)$  from the previous step  $k-1$ . This is done in the memory step. More precisely, the kernel weights  $W_{u,\lambda}^{(k,T)}(s, j)$  for the estimator  $\hat{f}_T^{(k)}(u, \lambda)$  in (3.7) are given by the linear combination

$$W_{u,\lambda}^{(k,T)}(s, j) = (1 - \theta_{u,\lambda}^{(k)}) \tilde{W}_{u,\lambda}^{(k,T)}(s, j) + \theta_{u,\lambda}^{(k)} W_{u,\lambda}^{(k-1,T)}(s, j). \quad (3.11)$$

Similarly, the effective sum of weights is given recursively by  $N_{u,\lambda}^{(k,T)} = (1 - \theta_{u,\lambda}^{(k)}) \tilde{N}_{u,\lambda}^{(k,T)} + \theta_{u,\lambda}^{(k)} N_{u,\lambda}^{(k-1,T)}$ . Here,  $\theta_{u,\lambda}^{(k)}$  takes values in  $[0, 1]$  based on the difference between the auxiliary estimator  $\tilde{f}_T^{(k)}(u, \lambda)$  and the previous estimator  $\hat{f}_T^{(k-1)}(u, \lambda)$ . The more the two estimators differ the more weight is given to the previous estimate. This ensures a smooth transition of the estimators between iteration steps and prevents the algorithm from gradually accumulating estimation errors. This memory-step is essential in the current setting of time-varying spectral densities that exhibit smooth changes in both time- and frequency direction. Although (Polzehl and Spokoiny 2006) also consider a memory step to allow for smoother changes, in our case it also plays a crucial role in reducing the effect of cross-interference terms. We discuss this in more detail in section 3.5.

### 3.4. Penalty step

The penalty statistic underlying the penalty kernel is an essential part of the procedure. At each iteration, it determines in which direction and to what degree smoothing occurs. We motivate the construction of our statistic as follows. In case the true spectrum is flat, the statistic must be such that no actual penalization occurs and by the end of the procedure our adaptive estimates ought to coincide with nonadaptive estimates obtained with global bandwidths  $b_t = 1$  and  $b_f = 2\pi$ . In other words, free extension of the smoothing bandwidths over the entire time-frequency plane should imply a completely homogeneous true spectrum. The scenario we are interested in is therefore whether two spectral estimates at different points can be considered to belong to the same 'homogeneous' region. In order to construct the test statistic we note that for the nonadaptive estimator given in (3.6), we have under certain regularity conditions (section 3.8), the following result:

$$T b_{t,T} b_{f,T} \left( \hat{f}_T(u_1, \lambda_1) - f(u_1, \lambda_1) \right)^2 \xrightarrow{\mathcal{D}} 2\pi \kappa_t \kappa_f f^2(u_1, \lambda_1) \chi_1^2, \quad (3.12)$$

where  $\kappa_t = \int K_t^2(x)dx$  and  $\kappa_f = \int K_f^2(x)dx$ . This implies

$$T b_{t,T} b_{f,T} (\hat{f}_T(u_1, \lambda_1) - \hat{f}_T(u_2, \lambda_2))^2 \xrightarrow{\mathcal{D}} 4\pi \kappa_t \kappa_f f^2(u_1, \lambda_1) \chi_1^2, \quad (3.13)$$

if homogeneity is satisfied. The latter result will be used as a general guideline to determine the degree of smoothing. More specifically, when constructing the new weights for the estimator at point  $(u_1, \lambda_1)$ , the result in (3.13) can be applied to ‘test’ if  $\hat{f}_T(u_2, \lambda_2)$  belongs to the confidence interval of  $\hat{f}_T(u_1, \lambda_1)$ .

**3.4.1. Penalty statistic.** The result in (3.13) motivates to consider a penalty statistic given by

$$P^{(k+1,T)}((u_1, \lambda_1), (u_2, \lambda_2)) = \frac{\tilde{N}_{u_1, \lambda_1}^{(k,T)}}{2\pi \kappa_f \kappa_t T} \left( \frac{\hat{f}_T^{(k)}(u_1, \lambda_1) - \hat{f}_T^{(k)}(u_2, \lambda_2)}{\bar{f}_T^{(k)}(u_1, \lambda_1)} \right)^2. \quad (3.14)$$

Here, the factor  $\tilde{N}_{u_1, \lambda_1}^{(k,T)}$  measures the bandwidth of the adaptive kernel, e.g., for a nonadaptive kernel we would have  $2\pi \tilde{N}_{u_1, \lambda_1}^{(k,T)} \approx b_{t,T} b_{f,T} T^2$ . If the value of the penalty statistic is close to zero and  $\hat{f}_T^{(k)}(u_2, \lambda_2)$  can be considered to belong to the same region as  $\hat{f}_T^{(k)}(u_1, \lambda_1)$ , then the penalty kernel provides full weight to the corresponding pre-periodogram variate  $J_T(u_2, \lambda_2)$  in the construction of the new estimator  $\tilde{f}_T^{(k+1)}(u_1, \lambda_1)$ . As in the nonadaptive case, it will then only be down weighted based on its absolute distance to the current point of interest by means of the kernels  $K_{f,T}$  and  $K_{t,T}$ . From (3.14), it is easily observed that as the effective sum of weights increases and hence variability decreases, penalization becomes more severe. Moreover, it can be seen that this statistic is not symmetric but is based on the values of  $N^{(k,T)}$  and  $\bar{f}_T^{(k)}$  evaluated only around the point of interest, in this case  $(u_1, \lambda_1)$ . The reason is that for the type of processes we are interested in, i.e., smooth spectra with possible breaks, homogeneity is in general only a meaningful concept at a local level. In practice, we therefore need to take into account that energy levels differ over the plane. An important part of our algorithm is therefore the construction of the term  $\bar{f}_T^{(k)}(u_1, \lambda_1)$ , which replaces the denominator and takes into account the local energy- and noise level.

**3.4.2. Construction of the denominator.** More specifically, the unknown spectral density in the denominator has been replaced by

$$\bar{f}_T^{(k)}(u_1, \lambda_1) = \overline{\hat{f}_T^{(k)}}(u_1, \lambda_1) + \hat{\sigma}_T^{(k)}(u_1, \lambda_1). \quad (3.15)$$

Here,

$$\overline{\hat{f}_T^{(k)}}(u_1, \lambda_1) = \frac{1}{N^*} \sum_{s,j} |\hat{f}_T^{(k)}(\frac{s}{T}, \lambda_j)| 1_{\{|s/T - u_1| \leq b_{t,T}^{(k)*}, |\lambda_j - \lambda_1| \leq b_{f,T}^{(k)*}\}} \quad (3.16)$$

with  $N^* = \sum_{s,j} 1_{\{|s/T - u_1| \leq b_{t,T}^{(k)*}, |\lambda_j - \lambda_1| \leq b_{f,T}^{(k)*}\}}$  defines the local mean level over the neighborhood of  $(u_1, \lambda_1)$  defined by the bandwidths  $b_{f,T}^{(k)*}$  and  $b_{t,T}^{(k)*}$ . Correspondingly,

$$\hat{\sigma}_T^{(k)}(u_1, \lambda_1)^2 = \frac{1}{N^*} \sum_{s,j} [\hat{f}_T^{(k)}(\frac{s}{T}, \lambda_j) - \overline{\hat{f}_T^{(k)}}(u_1, \lambda_1)]^2 1_{\{|s/T - u_1| \leq b_{t,T}^{(k)*}, |\lambda_j - \lambda_1| \leq b_{f,T}^{(k)*}\}}, \quad (3.17)$$

denotes the local variation about the local mean level over the same neighborhood. The motivation behind expression (3.15) is directly related to the iterative nature

of the procedure and the underlying raw estimator. In particular, the method must not be too sensitive in areas with low signal to noise ratios and when the plane exhibits fast changes or high levels of curvature. The term (3.15) controls for this and we shall discuss the role of its respective two components in turn.

- (i) **Local average**  $\overline{\hat{f}_T^{(k)}}(u_1, \lambda_1)$ : Since (3.15) is replacing the true spectrum at point  $(u_1, \lambda_1)$  it needs to be representable for the local level of energy. Instead of replacing it with the point estimator, we use a local average as given in (3.16). The main reason is that we require it to be a stable representative value for the level of energy not only *at* the point of interest but also in a direct neighborhood around the point. If two adjacent points  $\hat{f}_T^{(k)}(u_i, \lambda_i)$ ,  $i = 1, 2$ , have very different energy levels and the denominator of the corresponding statistics  $P^{(k+1,T)}((u_1, \lambda_1), (u_2, \lambda_2))$  and  $P^{(k+1,T)}((u_2, \lambda_2), (u_1, \lambda_1))$  are very different, the values of these statistics will also differ substantially. Consequently, the corresponding weights in their respective updated estimates for step  $k + 1$  will also be quite different. Especially in areas with high curvature, this could result in wrongful separation as the procedure continues. To make the method more robust against too early separation, we thus average locally in such a way that (3.16) is a reasonably smooth function over the plane.
- (ii) **Local noise measure**  $\hat{\sigma}_T^{(k)}(u_1, \lambda_1)$ : By definition, it gives a measure of local variation about the local mean level of energy in the neighborhood. A high value indicates that the local average (3.16) is off with respect to the actual level of energy directly at the point of interest  $(u_1, \lambda_1)$ . Accordingly, such a high value will result in less severe penalization by (3.15). This is of essence at the beginning of the procedure when the estimated plane is suffering from more noise as well as when local homogeneity starts to get violated and effective bandwidths and consequently noise levels start to differ. It then facilitates the possibility that optimal effective bandwidths might be reached earlier in certain areas while in others smoothing could still yield considerable improvement.

**Remark 3.1.** Note moreover that the local average in (3.16) is taken over the absolute set of estimates. This ensures that regions in which negative estimates occur, caused by the cross-interference terms underlying the pre-periodogram, are not over penalized. This feature, together with the memory step and the adjusted pre-periodogram (3.4), allows our method to reduce the effect of cross-interference terms to a minimum.

In the neighborhood of a break in the spectrum, the denominator term (3.15) will also take larger values. Nevertheless, breaks are still detected by our method if they locally dominate the smooth changes. In that case, the difference term in the nominator in (3.14) will approximately stay constant for two points on either side of the break whereas the total weight  $N_{u,\lambda}^{(k,T)}$  of the kernels increases with  $k$  and thus leads to effective penalization of all values on the opposite side of the break. Consequently, all weight of the kernel given by  $\tilde{W}_{u,\lambda}^{(k+1,T)}$  is distributed to those values that are on the same side of the break as  $(u, \lambda)$ . In contrast, if the spectral density is smooth in the neighborhood of the point  $(u, \lambda)$ , the difference in the nominator in (3.14) changes only gradually as points further away from  $(u, \lambda)$  are considered. This

leads to penalization kernels that decay smoothly and change smoothly between points. A large value of  $\hat{\sigma}_T^{(k)}(u_1, \lambda_1)$  will then delay strong penalization and thus facilitates further propagation. The effect of  $\hat{\sigma}_T^{(k)}(u_1, \lambda_1)$  on the penalization statistic is negligible in case the plane exhibits local homogeneity. In order to reduce its importance if this is violated, the bandwidths  $b_{f,T}^{(k)*}$  and  $b_{t,T}^{(k)*}$  are reduced iteratively at a rate that is proportional to the rate at which the effective bandwidth grow. In areas where local homogeneity is not satisfied, this ensures that in later stages of the algorithm  $\bar{f}_T^{(k)}(u_1, \lambda_1)$  is converging to the actual level of energy at the point of interest  $(u_1, \lambda_1)$ .

**Remark 3.2 (An alternative statistic).** To avoid the problem of standardization, we additionally investigated a log version of the statistic given by

$$P_{II}^{(k+1,T)}((u_1, \lambda_1), (\lambda_2, \lambda_2)) = \frac{N_{u_1, \lambda_1}^{(k,T)}}{2\pi\kappa_t\kappa_f T} \left( \log(\hat{f}_T^{(k)}(u_1, \lambda_1)) - \log(\hat{f}_T^{(k)}(u_2, \lambda_2)) \right)^2. \quad (3.18)$$

Since the spectral density in the asymptotic variance cancels when considering log-ratios, the statistic does not require normalization by the unknown spectral density and thus is symmetric. The advantage is that less parameters need to be specified and the estimation method is simpler. However, the highly volatile behavior of the pre-periodogram and the possibility of negative estimates makes this version more problematic. For the log statistic it is essential to bound the initial estimates sufficiently far away from zero, while our original can deal with possible negative values. Moreover, it does not provide the same data-driven adaptation to local characteristics that allows for both smoothness and breaks. More details on this version are available upon request.

### 3.5. The memory step

Another important aspect of our procedure is the memory step which takes care of two problems. Firstly, it controls for the ‘bad’ behavior of the pre-periodogram. Secondly, it controls for accumulation of errors in areas where the spectrum is only gradually changing. In such regions, the adaptive bandwidths can increase even though the assumption of homogeneity has been violated. The larger neighborhood usually first leads to a drop in the estimation error but after some iteration the violation will result in an increasingly larger error which is carried over to next iterations. Imposing memory ensures that estimation precision reached in preceding iterations does not get lost and is used to bias, to some extent, the smoothing kernel to stability.

During the step, the new estimator  $\hat{f}_T^{(k)}(u, \lambda)$  is constructed by shifting the auxiliary estimator  $\tilde{f}_T^{(k)}(u, \lambda)$  towards the estimator  $\hat{f}_T^{(k-1)}(u, \lambda)$  from the previous iteration. The size of the shift depends on the difference of the auxiliary and the previous estimator. More precisely, the shift is determined by  $\theta_{u,\lambda}^{(k)}$ , which is given by

$$1 - \theta_{u,\lambda}^{(k)} = (1 - \eta) K_{\text{mem}} \left( P_{\text{mem}}^{(k,T)}(u, \lambda) \right) \quad (3.19)$$

and defines the actual amount of memory.  $\theta_{u,\lambda}^{(k)}$  takes values in  $[\eta, 1]$ , where the constant  $\eta \in [0, 1]$  specifies the minimal amount of memory imposed on the procedure.

Furthermore,  $K_{\text{mem}}(x)$  is a kernel that is monotonically decreasing for  $x \geq 0$  with  $K(0) = 1$ . Similar to the penalty statistic, we consider

$$P_{\text{mem}}^{(k,T)}(u, \lambda) = \frac{N_{u,\lambda}^{(k,T)}}{2\pi\kappa_t\kappa_f T} \left( \frac{\tilde{f}_T^{(k)}(u, \lambda) - \hat{f}_T^{(k-1)}(u, \lambda)}{\tilde{f}_T^{(k)}(u, \lambda)} \right)^2. \quad (3.20)$$

The term  $\tilde{f}_T^{(k)}(u, \lambda)$  in the denominator is defined as in the penalty step but may be based on a smaller neighborhood (specified by bandwidths  $b_{t,T}^{(k)**}$  and  $b_{f,T}^{(k)**}$ ) about the point  $(u_1, \lambda_1)$ . The new effective estimate  $\hat{f}_T^{(k)}(u_1, \lambda_1)$  is then obtained by a linear combination of the kernel weights for the auxiliary estimator  $\tilde{f}_T^{(k)}(u, \lambda)$  and the previous estimator  $\hat{f}_T^{(k-1)}(u, \lambda)$ , i.e.,

$$W_{u,\lambda}^{(k,T)}(s, j) = (1 - \theta_{u,\lambda}^{(k)}) \tilde{W}_{u,\lambda}^{(k,T)}(s, j) + \theta_{u,\lambda}^{(k)} W_{u,\lambda}^{(k-1,T)}(s, j). \quad (3.21)$$

Similarly, the total sum of effective kernel weights is given by  $N_{u,\lambda}^{(k,T)} = (1 - \theta_{u,\lambda}^{(k)}) \tilde{N}_{u,\lambda}^{(k,T)} + \theta_{u,\lambda}^{(k)} N_{u,\lambda}^{(k-1,T)}$ . The new estimator in terms of the auxiliary estimator and previous estimator can thus be given by

$$\hat{f}_T^{(k)}(u_1, \lambda_1) = \frac{(1 - \theta_{u,\lambda}^{(k)}) \tilde{f}_T^{(k)}(u, \lambda) + \theta_{u,\lambda}^{(k)} \hat{f}_T^{(k-1)}(u, \lambda)}{(1 - \theta_{u,\lambda}^{(k)}) \tilde{N}_{u,\lambda}^{(k,T)} + \theta_{u,\lambda}^{(k)} N_{u,\lambda}^{(k-1,T)}}. \quad (3.22)$$

If the value of the penalty is big,  $\theta^{(k)}$  will be large and hence more weight is given to the previous update allowing to retain estimation accuracy obtained in the preceding steps. The higher the value of  $\eta$  the more smooth the transition between old and new updates. At the same time, in case the changes are not gradual but rather strong discontinuities are present, higher values of  $\eta$  will slow down how fast a certain level of precision is reached. As we require a balance between smooth transitions and the possibility of breaks it should not be set too high. We recommend  $\eta \leq 0.25$ . Subsequent updates of the same point as used in the memory penalty statistic are not independent and are expected to get more correlated as iterations continue. We take this into account by penalizing more severely as  $k$  increases by using the adaptive (bigger) sum of weights belonging to the new adaptive estimate as given by  $N_{u,\lambda}^{(k,T)}$  and a much lower cut-off value. Note moreover that as long as the growth rates are set high enough, the level of correlation can be managed. We will explain this in more detail in section 4.

**Remark 3.3 (Controlling for cross-interference terms).** Besides from reducing accumulation of estimation errors, the memory step is crucial in controlling for possible negative initial estimates caused by cross-interference terms present in the pre-periodogram. In order to retrieve localized features, it is best to keep the initial bandwidths as small as possible. This means the initial estimates are affected by cross-interference terms and hence can be negative. The memory step enables to remove these iteratively. This is done by imposing full memory in case the new update is more negative than its previous value. Together with the construction of the denominator of the penalty step, this leads them to be gradually pushed towards a positive value and prevents the rest of the plane to be affected.

**Remark 3.4.** We note that in our case the memory step is an essential part of the procedure both to control for this ‘bad’ behavior of the underlying pre-periodogram and the local slowly changing dynamics in the spectrum. This in contrast to Becker and Mathé (2013) who consider piecewise constant functions in the time-domain and conclude such a relaxation step is redundant in their case.

### 3.6. The procedure

We now turn to the procedure in which we distinguish between the fully adaptive and the effective parameters/estimators by providing them with a tilde  $\tilde{\cdot}$  and a hat  $\hat{\cdot}$  respectively. The complete procedure is then as follows:

1. **Select parameters:** the bandwidth parameters  $b_{t,T}^{(0)}, b_{f,T}^{(0)}, \gamma_t, \gamma_f, k_{\max}$  (start, growth rates, maximum number of iterations). Moreover, we will need to set the parameters  $b_{t,T}^{(k)*}, b_{f,T}^{(k)*}$  and  $b_{t,T}^{(k)**}, b_{f,T}^{(k)**}$  for the penalty- and memory statistic, respectively. For ease of exposition, we will postpone specification of the parameters to section 4.

Then for all  $u = \frac{t}{T}, \lambda = \lambda_i$  in the time-frequency plane:

2. **Initialisation:** Construct the initial set of weights

$$W_{u,\lambda}^{(\text{in},T)}(s,j) = \frac{1}{b_{f,T}^{(0)}} K_f\left(\frac{\lambda - \lambda_j}{b_{f,T}^{(0)}}\right) \frac{1}{b_{t,T}^{(0)}} K_t\left(\frac{u - \frac{s}{T}}{b_{t,T}^{(0)}}\right) \quad (3.23)$$

and construct the initial set of estimates, denoted by  $\hat{f}_T^{\text{in}}(u, \lambda)$ . Using these, construct the first set of fully adaptive weights  $\{(s, j) : \tilde{W}_{u,\lambda}^{(0,T)}(s, j)\}$  and estimates  $\tilde{f}_T^{(0)}(u, \lambda)$  and accordingly the effective estimates  $\hat{f}_T^{(0)}(u, \lambda)$  and sum of weights  $N_{u,\lambda}^{0,T}$  by following step 3 and 4 below. Set  $k = 1$ .

3. **Penalty step:** Compute the value of the penalty statistic based on the effective estimates  $\hat{f}_T^{(k-1)}$  of the previous step. That is, compute

$$P^{(k,T)}[(u, \lambda), (\frac{s}{T}, \lambda_j)] \quad (3.24)$$

using (3.14) and accordingly the corresponding adaptive weights

$$\tilde{W}_{u,\lambda}^{(k,T)}(s,j) = K_f\left(\frac{\lambda - \lambda_j}{\tilde{b}_{f,T,u,\lambda}^{(k)}}\right) K_t\left(\frac{u - \frac{s}{T}}{\tilde{b}_{t,T,u,\lambda}^{(k)}}\right) K_p\left(P^{(k,T)}[(u, \lambda), (\frac{s}{T}, \lambda_j)]\right), \quad (3.25)$$

in order to construct the fully adaptive estimator  $\tilde{f}_T^{(k)}(u, \lambda)$ .

4. **Memory step:** Compare  $\tilde{f}_T^{(k)}(u, \lambda)$  with  $\hat{f}_T^{(k-1)}(u, \lambda)$ , the previous effective estimate based on the memory penalty statistic  $P_{\text{mem}}^{(k)}(u, \lambda)$  as defined in (3.20) and compute the effective set of weights

$$W_{u,\lambda}^{(k,T)}(s,j) = (1 - \theta_{u,\lambda}^{(k)}) \tilde{W}_{u,\lambda}^{(k,T)}(s,j) + \theta_{u,\lambda}^{(k)} W_{u,\lambda}^{(k-1,T)}(s,j) \quad (3.26)$$

and effective estimate

$$\hat{f}_T^{(k)}(u_1, \lambda_1) = \frac{(1 - \theta_{u,\lambda}^{(k)}) \tilde{f}_T^{(k)}(u, \lambda) + \theta_{u,\lambda}^{(k)} \hat{f}_T^{(k-1)}(u, \lambda)}{(1 - \theta_{u,\lambda}^{(k)}) \tilde{N}_{u,\lambda}^{(k,T)} + \theta_{u,\lambda}^{(k)} N_{u,\lambda}^{(k-1,T)}}. \quad (3.27)$$

Set  $k = k + 1$ .

**5. Stopping rule:** Repeat steps 3 and 4 until  $k = k_{\max}$ .

**Remark 3.5.** In order to obtain the first set of fully adaptive estimates  $\{(u, \lambda) : \tilde{f}_T^{(0)}(u, \lambda)\}$ , the penalty statistic is based on the initial set of nonadaptive estimates  $\{(u, \lambda) : \hat{f}_T^{\text{in}}(u, \lambda)\}$ . The first set of effective estimates  $\{(u, \lambda) : \hat{f}_T^0(u, \lambda)\}$  are then obtained by applying the memory statistic to  $\tilde{f}_T^{(0)}(u, \lambda)$  and  $\hat{f}_T^{\text{in}}(u, \lambda)$  for all  $u, \lambda$ .

### 3.7. Computational complexity

The algorithm has been implemented in R using the **Rcpp** package in order to make use of the compiler language C++. In particular, certain parts of the algorithm are implemented using the OpenMP interface for carrying out parallel computations in a shared memory environment. The reason for this is the complexity of the algorithm. For a time-series of length  $T$ , the time-frequency plane will consist of  $T^2$  data-points. Using the FFT algorithm, computing the pre-periodogram variates is an operation of order  $O(T \ln(T))$ . The computational cost lies however in the quantity of weights to construct. In step  $k$ , the maximum number of weights to compute for the new estimator of step  $k + 1$ , will approximately be between  $\frac{3}{8\pi} b_{t,T}^{(0)} \gamma_t^{(k+1)} b_{f,T}^{(0)} \gamma_f^{(k+1)} T^2$  and  $\frac{1}{2\pi} b_{t,T}^{(k+1)} \gamma_t^{(k+1)} b_{f,T}^{(0)} \gamma_f^{(k+1)} T^2$ , depending on whether we are in the middle of the plane or at the boundaries. Determining a weight value, i.e., constructing the kernel values, and additionally the sums of weights is an operation of order  $O(1)$ . The maximum complexity of the construction for the new estimator at one particular point is therefore of order  $O(b_{t,T}^{(k+1)} b_{f,T}^{(k+1)} T^2)$ . It follows that the total complexity of the algorithm is  $O(b_{t,T}^{(k_{\max})} b_{f,T}^{(k_{\max})} T^4)$ . We remark however that for most points in the plane, the final effective bandwidths  $\tilde{b}_{t,T,u,\lambda}^{(k_{\max})}$  and  $\tilde{b}_{f,T,u,\lambda}^{(k_{\max})}$ , which are computed using (3.10), will be much lower than  $b_{t,T}^{(0)} \gamma_t^{(k_{\max})}$  and  $b_{f,T}^{(0)} \gamma_f^{(k_{\max})}$ .

### 3.8. Asymptotic considerations

The objective of this section is to provide some intuition on the distributional properties of the adaptive estimator in (3.8). We do this in the setting of empirical spectral processes (e.g. Dahlhaus and Polonik 2009, Dahlhaus 2009), on which we first provide some background. Generally, the empirical spectral process for arbitrary index functions  $\phi$  is defined by

$$E_T(\phi) = \sqrt{T}(F_T(\phi) - F(\phi)), \quad (3.28)$$

where

$$F(\phi) = \int_0^1 \int_{-\pi}^{\pi} \phi(u, \lambda) f(u, \lambda) du d\lambda \quad (3.29)$$

is the generalized spectral measure and

$$F_T(\phi) = \frac{1}{T} \sum_{t=1}^T \int_{-\pi}^{\pi} \phi\left(\frac{t}{T}, \lambda\right) J_T\left(\frac{t}{T}, \lambda\right) d\lambda \quad (3.30)$$

denotes the corresponding empirical spectral measure. For particular classes of index functions independent of  $T$ , a functional central limit theorem has been proved (Dahlhaus and Polonik 2009, Theorem 2.11). Additionally, for index functions depending on  $T$  a central limit theorem has been derived (Dahlhaus 2009, Theorem

3.2). Both results are shown under the following conditions on the corresponding stochastic process. Here, let

$$V(g) = \sup_{0 \leq y_0 \leq \dots \leq y_m \leq 1, m \in \mathbb{N}} \sum_{k=1}^m |g(y_k) - g(y_{k-1})|, \quad (3.31)$$

denote the total variation of a function  $g$  on  $[0, 1]$  and let  $l(j) = \max\{1, |j| \log^{1+\varsigma} |j|\}$  for some  $\varsigma > 0$ .

**Assumption 3.6.**  $\{X_{t,T}\}$  is locally stationary according to Definition 2.1 such that the coefficients  $a_{t,T}(j)$ ,  $j \in \mathbb{N}$  of the linear filter defined by the transfer function  $A_{t,T}(\lambda)$  satisfy

$$\sup_{t,T} |a_{t,T}(j)| \leq \frac{C}{l(j)}, \quad (3.32)$$

for some constant  $C$  not depending on  $T$ . Moreover, the coefficients  $a(u, j)$ ,  $j \in \mathbb{N}$ , of the linear filter defined by the transfer function  $A(u, \lambda)$  satisfy

$$\sup_{u \in [0,1]} |a(u, j)| \leq \frac{C}{l(j)}, \quad (3.33)$$

$$\sup_{j \in \mathbb{N}} \sum_{t=1}^T |a_{t,T}(j) - a(\frac{t}{T}, j)| \leq C, \quad (3.34)$$

$$V(a(\cdot, j)) \leq \frac{C}{l(j)}. \quad (3.35)$$

Many localized statistics for non-stationary time series can be written in terms of the empirical spectral measure. In particular, we obtain the non-adaptive time-varying spectral estimator in (3.5) by considering index functions

$$\phi_{u,\lambda}^{(T)}(v, \mu) = \frac{1}{b_{t,T} b_{f,T}} K_t\left(\frac{u-v}{b_{t,T}}\right) K_f\left(\frac{\lambda-\mu}{b_{f,T}}\right). \quad (3.36)$$

Since the index functions depend on  $T$ , asymptotic normality of the estimator  $F_T(\phi_{u,\lambda}^{(T)})$  and its discretized version (3.6) follows from Theorem 3.2 and Example 4.1 of Dahlhaus (2009) under the following additional conditions.

**Assumption 3.7.**

- (i) The time-varying spectral density  $f(u, \lambda)$  is twice differentiable in  $u$  and  $\lambda$  with uniformly bounded derivatives.
- (ii) The bandwidths satisfy  $b_{t,T}, b_{f,T} \rightarrow 0$  and  $b_{t,T} b_{f,T} T \gg \log(T)^2$  as  $T \rightarrow \infty$ ,
- (iii) The kernels  $K_t$  and  $K_f$  are of bounded variation with compact support. Moreover,  $\int x K_t(x) dx = 0$  and  $\int K_t(x) dx = 1$  and analogously for  $K_f$ .

In particular, we find that

$$b_{t,T} b_{f,T} \text{var}(E_T(\phi_{u,\lambda}^{(T)})) \rightarrow 2\pi f(u, \lambda) \kappa_t \kappa_f.$$

Furthermore, estimators at different points in the time-frequency plane are asymptotically independent.

For the adaptive estimator in (3.8) similar asymptotic results cannot be derived easily since the final smoothing kernel is iteratively defined and depends on the spectral estimators in previous steps through penalization and the memory step. In the following, we therefore provide at least heuristic arguments that under homogeneity of the spectral density penalization has a negligible effect and hence the estimator remains consistent and asymptotically normal.



More precisely assume that  $f(u, \lambda) = f$  for all  $u$  and  $\lambda$  and define for fixed  $u \in [0, 1]$  and  $\lambda \in [-\pi, \pi]$  the functions

$$\psi_{\alpha, \beta} = \phi_{u+\alpha b_{t,T}, \lambda+\beta b_{f,T}}^{(T)} \quad (3.37)$$

where  $\phi_{u, \lambda}^{(T)}$  is defined as above. Then the family of index functions  $\mathcal{F}_0 = \{\psi_{\alpha, \beta} | \alpha, \beta \in [-1, 1]\}$  satisfies the conditions of Theorem 2.11 of Dahlhaus and Polonik (2009). Hence the penalty statistic  $P^{(k, T)}[(u, \lambda), (u + \alpha b_{t,T}, \mu + \beta b_{f,T})]$  asymptotically has that same distribution as

$$\frac{b_{t,T} b_{f,T}}{2\pi \kappa_f \kappa_t f^2} (E(\psi_{0,0}) - E(\psi_{\alpha, \beta}))^2,$$

where  $E(\psi)$  is a Gaussian process with mean zero and covariances

$$\begin{aligned} b_{t,T} b_{f,T} \text{cov}(E(\psi_{\alpha, \beta}), E(\psi_{\gamma, \delta})) &= 2\pi f^2 \int_{-1/2}^{1/2} \int_{-\pi}^{\pi} K_t(\alpha - u) K_t(\gamma - u) K_f(\beta - \lambda) \\ &\quad \times [K_f(\delta - \lambda) + K_f(\delta + \lambda)] du d\lambda + O(b_{f,T}). \end{aligned}$$

The expression shows that under the assumption of homogeneity of the time-varying spectrum over the local neighborhood about the point  $(u, \lambda)$  the distribution of the penalty statistic does not depend on the bandwidth or the sample size but through a term of order  $O(b_{f,T})$ . Moreover, the strong positive correlation of the Gaussian process  $E(\psi)$  leads to at most weak penalization towards the borders of the local neighborhood yielding a total smoothing kernel that differs only slightly from the non-adaptive smoothing kernel. Finally, since  $E(\psi_{0,0})$  and  $E(\psi_{\alpha, \beta})$  are positively correlated, the variance of their difference can be bounded by  $2 \text{var}(E(\psi_{0,0}))$  uniformly for all  $\alpha, \beta \in [-1, 1]$ , which justifies the use of (3.13) for determining the cut-off point of the penalty kernel.

We note that the same covariance structure can be derived from Theorem 3.2 of Dahlhaus (2009) by considering the index functions  $\phi_{u+\alpha b_{t,T}, \lambda+\beta b_{f,T}}^{(T)}$  directly, that is, taking their dependence on  $T$  into account in the asymptotics. However, the result is weaker insofar it does not yield convergence over the whole local neighborhood defined by  $\alpha, \beta \in [-1, 1]$  simultaneously. Although the above arguments based on fixed index functions indicate that this result could be strengthened, a derivation of a functional central limit theorem in this setting is beyond the scope of this paper.

Summarizing we find that under the assumption of homogeneity penalization does only modify the shape of the smoothing kernel even if applied iteratively multiple times but will keep the rates approximately the same. In contrast, in case of a non-constant spectral density, the penalty statistic depends quadratically on the difference in levels which leads to more severe penalization as bandwidths in time and frequency direction increase. Accordingly, the resulting smoothing kernel will have in general a smaller support corresponding to a smaller bandwidth than the one actually imposed. Nevertheless, in the setting of locally stationary processes this effect will disappear asymptotically since the level of local homogeneity increases as long as the bandwidths used in the iteration satisfy the conditions in Assumption 3.7. In other words, the adaptive estimator remains consistent with rate  $\sqrt{T b_{t,T}^{(k_{\max})} b_{f,T}^{(k_{\max})}}$  since its adaptiveness only shows in finite samples. This is even true when the dynamics of the process exhibits structural breaks and thus should be described by

a piecewise locally stationary process. In that case, penalization will be strong in the local neighborhood of a break leading to asymmetric smoothing kernels that seem to be cut off. Again, since the local neighborhoods (in the rescaled time–frequency plane) are shrinking for increasing sample size, the effect will disappear but for the points along the breaks where the time–varying spectral density is not well–defined. Examples of such processes with structural breaks will be discussed in Section 5, where we illustrate the final sample behavior of the adaptive estimator by simulations.

**3.8.1. Bias.** Under assumption 3.7, it is easily derived that the bias under local homogeneity can approximately be given by

$$\frac{1}{2} b_{t,T}^{(k)2} \int x^2 K_t(x) dx \frac{\partial^2}{\partial u^2} f(u, \lambda) + \frac{1}{2} b_{f,T}^{(k)2} \int x^2 K_f(x) dx \frac{\partial^2}{\partial \lambda^2} f(u, \lambda) + o(1), \quad (3.38)$$

and thus will be negligible for bandwidths satisfying

$$\sqrt{T b_{t,T}^{(k)} b_{f,T}^{(k)} (b_{t,T}^{(k)2} + b_{f,T}^{(k)2})} \rightarrow 0 \text{ as } T \rightarrow \infty.$$

In the asymptotics, this needs to be balanced with the other assumption on the bandwidths underlying the central limit theorem (Assumption 3.7(ii)) and constitutes the usual bias–variance trade–off. When  $T$  is fixed, the bias present in  $\hat{f}_T^{(k)}(u_1, \lambda_1)$  and  $\hat{f}_T^{(k)}(u_2, \lambda_2)$  cancels out in the penalty statistic under local homogeneity. Moreover, in case the bias starts to differ either due to differences in effective bandwidths or a difference in curvature, then this be detected by the penalty statistic through  $\tilde{\sigma}_T^{(k)}(u_1, \lambda_1)$  or  $\tilde{\sigma}_T^{(k)}(u_2, \lambda_2)$ , translating in a higher value of (3.15) and in turn reducing the risk of wrongful rejection due to difference in bias. Because of this property of the penalty statistic to adjust to bias, taking into account 3.7(ii) will be of more importance when specifying the initial bandwidths  $b_{t,T}^{(0)}$  and  $b_{f,T}^{(0)}$ , than the bias criteria.

## 4. SPECIFICATION OF PARAMETERS

In this section, we discuss some guidelines on how to set the parameters of the procedure. As long as these guidelines are followed our method is robust under different processes and additional fine-tuning is not necessary.

### 4.1. Bandwidth parameters

**4.1.1. Initial bandwidths.** It is clear that the smaller the initial bandwidth the more details can be retrieved. This is however under the constraint that the initial set of nonadaptive estimates are not dominated by the variability and, in particular cross-interference terms, of the underlying pre–periodogram as they need to be stable enough to be used in the penalty statistic. The guideline is therefore to take the smallest bandwidths for which the smoothed pre–periodogram obeys the condition underlying the central limit theorem 3.7(iv);  $b_{t,T}^{(0)} b_{f,T}^{(0)} T \gg \log(T)^2$ . For example, when  $T = 512$ , we set  $b_{t,T}^{(0)} \approx 0.12$ ,  $\frac{1}{2\pi} b_{f,T}^{(0)} \approx 0.12$ , which can be reduced for larger values of  $T$ .

For the additional bandwidth parameters required for the penalty statistics (3.14) and (3.20), respectively, we set  $b_{t,T}^{(k)*} = b_{t,T}^{(k)**} = b_{t,T}^{(0)}$ ,  $b_{f,T}^{(k)*} = b_{f,T}^{(k)**} = b_{f,T}^{(0)}$ . As explained in section 3.4.1, these are reduced over iterations based on the rate at which the effective bandwidth of the  $q$ -th percentile is growing with respect to the starting bandwidths. We recommend  $10 \leq q \leq 20$ , to make sure this decrease goes gradually and at the same time is not affected by possible negative estimates.

**4.1.2. Growth rates.** The growth rates determine how much 'localization' takes place. If bandwidths increase at a high rate, the effect of the penalty statistic becomes more pronounced and the transition between local homogeneous regions less smooth. If set too high, the procedure might overlook gradual change or interesting characteristics. For example, when a region with similar energy level is included in the new larger neighborhood we could miss some feature in between. This is to some extent corrected for by the two kernels that penalize distance but could occur when two small peaks of similar energy are close to each other or close to a large peak, a common problem in spectral density estimation.

A lower bound on the growth rates is necessary to control violation of the independence assumption underlying the asymptotic distribution of the penalty statistic. To give some intuition, consider the algorithm at step  $k$ . We have estimates  $\hat{f}_T^{(k-1)}(u_i, \lambda_j)$  for all  $(u_i, \lambda_j) \in U \times \Pi$  and the bandwidths are set to  $\tilde{b}_{t,T,u,\lambda}^{(k)} = \gamma_t b_{t,T,u,\lambda}^{(k-1)}$  and  $\tilde{b}_{f,T,u,\lambda}^{(k)} = \gamma_f b_{f,T,u,\lambda}^{(k-1)}$ . To compute the estimate  $\hat{f}_T^{(k)}(u_i, \lambda_j)$ , a new set of weights  $\{\tilde{W}_{u_i,\lambda_j}^{(k,T)}(s, l)\}$  is constructed by comparing the estimate  $\hat{f}_T^{(k-1)}(u_i, \lambda_j)$  with all other estimates  $\hat{f}_T^{(k-1)}(u_s, \lambda_l)$  that fall into the new search neighborhood as given by the larger bandwidths. If the growth rates only allow a small increase of this neighborhood compared to the previous step, underlying weight sets and hence pre-periodogram variates will strongly overlap with one another. These estimates are therefore expected to be highly correlated with the current point of interest  $\hat{f}_T^{(k-1)}(u_i, \lambda_j)$ . This increases the risk that  $P^{(k,T)}$  will redistribute weights within approximately the same area as in the previous step leading to falsely iterative exclusion of certain data-points. It is thus of importance that the growth rates are high enough to make sure that a large part of weights is based on points that did not overlap in the previous step to ensure independence can be considered reasonable. Results show that rates  $\gamma_t$  and  $\gamma_f$  that satisfy  $1.2 \leq \gamma_t \gamma_f \leq 1.5$  provide a good balance.

**4.1.3. Maximal number of iterations.** The maximal iteration  $k_{\max}$  is determined by two conditions. Firstly, the effective sum of weights needs to increase sufficiently compared to the previous effective sum of weights. This for the same reason as discussed above, i.e. to prevent the penalty statistic from reconsidering approximately the same areas as in the previous iterations. To measure this, denote

$$\gamma^{(k)}(u_i, \lambda_l) = N_{(u_i, \lambda_l)}^{(k,T)} / N_{(u_i, \lambda_l)}^{(k-1,T)}.$$

The condition we impose is that the average over the time-frequency plane of the effective growth rate given by

$$\bar{\gamma}^{(k)} = \frac{1}{T^2} \sum_{i,l} \gamma^{(k)}(u_i, \lambda_l)$$

satisfies  $\bar{\gamma}^{(k)} > (\gamma_t \gamma_f)^{0.25}$ . Once this is no longer satisfied the algorithm stops. Additionally, the effect of bias (Remark 3.8.1) in case of local stationarity needs to be taken into account. As a proxy to measure when it starts to play a role, we use

$$\min_{i,l} b_{T,u_i,\lambda_l}^{(k)} \approx T^{-1/6} \quad (4.1)$$

If the algorithm reaches such bandwidths, smoothing is stopped when the dispersion between the highest and lowest quartile of  $\gamma^{(k)}$  over the time-frequency plane is larger than 10 % of possible change, i.e.,

$$\mathcal{Q}_{\gamma^k}(0.75) - \mathcal{Q}_{\gamma^k}(0.25) > 0.1 \gamma_t \gamma_f$$

Together these two conditions allow the method to automatically take into account the possibility for spectra with very steep and localized features and on the other hand to continue smoothing in case of spectra with large stationary or flat regions. The condition that the algorithm is keeping track of is therefore

$$k_{\max} = \underset{k}{\operatorname{argmin}} \left( \left\{ \bar{\gamma}^{(k)} > (\gamma_t \gamma_f)^{0.25} \right\} \cup \left\{ \mathcal{Q}_{\gamma^k}(0.75) - \mathcal{Q}_{\gamma^k}(0.25) > 0.1 \gamma_t \gamma_f \mid \min_{i,l} b_{T,u_i,\lambda_l}^{(k)} \approx T^{-1/6} \right\} \right) \quad (4.2)$$

**Remark 4.1 (Growth rates in case of negative estimates).** As explained in Remark 3.3, the memory step imposes full memory in case the auxiliary estimate is more negative than the previous effective estimate. For these point estimates, we require a lower growth rate  $\rho$  for the new search area to make sure the cross-interference effect is smoothed out locally and not by ‘accident’. We advise  $1.01 \leq \rho \leq 1.03$  depending on the length of data.

## 4.2. Kernels

The penalty kernel should be a concave function that tapers off softly. This because, even though the algorithm makes sure that the separation property is satisfied (weights that were zero remain zero), it will not necessarily stop redistributing the weights within a region considered ‘homogeneous’. A very steep penalty kernel as used in Polzehl and Spokoiny (2006) pushes more and more weight in a smaller area. The kernels  $K_t(x)$  and  $K_f(x)$  would exaggerate this behavior. This is clearly not suitable in our application as it leads to piecewise constant areas in the estimated plane. Instead, we need ‘smooth’ rejection over iterations, i.e., as the effective bandwidths grow and variability is reduced, the effect of the penalty kernel becomes more important. To establish this, we use the concave function

$$K_p(x) = \left[ 1 - \left( \frac{x}{c\rho^k} \right)^2 \right] 1_{[0,c\rho^k]}(x), \quad (4.3)$$

where the cut-off point is given by  $c = 2\chi_{1,0.9}^2$  and is based on the asymptotic distribution of the penalty statistic under local homogeneity. The term  $\rho^k$ , controls

that for unstable areas affected by cross-interference terms (Remark 4.1) the effect of the penalty statistic in the weight distribution does not gain importance. We note that at the beginning of the procedure, the assumed independence underlying the asymptotic distribution as given in (3.13) will not truly hold for adjacent points due to the overlap of raw estimates. In general, this is not a problem but rather provides initial support around the midpoint. For the memory kernel we take the linear kernel

$$K_{\text{mem}}(x) = \left(1 - \frac{x}{c\rho^{-k}}\right) 1_{[0, \rho^{-k}c_{\text{mem}}]}(x), \quad (4.4)$$

where the default choice for the cutoff point is  $c_{\text{mem}} = 2\chi_{1,0.75}^2$ . We let the kernel decrease at a rate  $\rho^k$  as we expect more correlation between the new and old estimator as iterations continue, especially in areas affected by the cross-interference terms. For the distance kernels  $K_t$  and  $K_f$ , we use quadratic kernels

$$K_t(x) = K_f(x) = 6\left(\frac{1}{4} - x^2\right) 1_{[-0.5, 0.5]}(x), \quad (4.5)$$

which have been shown to yield the smallest mean squared error (Dahlhaus 1996a) in case the null of homogeneity is satisfied.

**Remark 4.2.** If it is suspected the length of the data is too short for the asymptotic distribution to be reasonable to use for the cut-off point, one can scale the statistics appropriately. The amount of scaling can be determined by the smallest constant such that the procedure returns close to nonadaptive estimates for a homogeneous spectrum with similar mean energy as the original process.

## 5. EXAMPLES

In this section we illustrate the proposed adaptive smoothing method by applying it to three examples that cover three types of situation: constant spectra with a structural break, smooth time-varying spectra, and time-varying spectra that also exhibit structural breaks. In all examples, we choose the same set of tuning parameters for the algorithm to demonstrate that the method is to some degree insensitive against choice of parameters.

In all examples, the sample length is  $T = 1024$  and the initial bandwidths for the localization kernels are  $b_{t,T}^{(0)} = b_{f,T}^{(0)}/2\pi = 0.1$ . The growth rates are set to  $\gamma_t = \gamma_f = 1.2$  and  $\rho = 1.02$ . The parameters for the penalty step and the memory step are  $b_{t,T}^{(k)*} = b_{t,T}^{(0)}$ ,  $b_{f,T}^{(k)*} = b_{f,T}^{(0)}$ ,  $q = 0.15$ ,  $\eta = 0.25$ . The parameters for the kernels are the default choices as explained in the previous section. The corresponding figures<sup>1</sup> are given in the appendix.

### 5.1. Structural break white noise

As a first example, we consider a break in a white noise series. That is, we consider the following model for the observations

$$X_{t,T} = Z_t 1_{\{t \leq t_0\}} + \sqrt{10} Z_t 1_{\{t > t_0\}}, \quad Z_t \stackrel{\text{iid}}{\sim} \mathcal{N}(0, 1) \quad (5.1)$$

<sup>1</sup>All data is available upon request.

with  $t_0 = 576$ . The corresponding time-varying spectral density is given by

$$f(u, \lambda) = \frac{1}{2\pi} 1_{\{u \leq t_0/T\}} + \frac{10}{2\pi} 1_{\{u > t_0/T\}}. \quad (5.2)$$

and is depicted in Figure 5.1 (a). Figure 5.1 (b) shows the corresponding pre-periodogram. Compared with the usual periodogram, it exhibits much more variation which completely blur the piecewise constant form of the density. The initial adaptive estimate for  $k = 0$  is given in Figure 5.1 (c). Here, the change in level is already discernible but the estimate is still relatively non-smooth. Following (4.2), the algorithm stopped at  $k_{\max} = 11$  iterations and yields the estimated time-frequency plane in Figure 5.1 (d). It clearly shows two levels for the spectral density. Figures 5.2 (a)–(b) depict, respectively, the final penalty and adaptive kernel for the mid-point of the plane. Once the break is detected the penalty kernel forces the weights down to zero. This results in asymmetric smoothing kernel that is ‘cut’ off and thus succeeds in separating the areas on both sides of the break. To demonstrate the effect of the procedure, figure 5.1 (e) shows the estimated plane using the non-adaptive estimator as given in (3.6) with the same total search neighborhood, i.e., with bandwidths  $\gamma_t^{11}$  and  $b_{t,T}^{(0)}, \gamma_f^{11} b_{f,T}^{(0)}$ . Not surprisingly, the presence of the break is completely smoothed out.

To benchmark how our method performs, we use a proxy for the optimal unknown global bandwidths for the nonadaptive estimator. To construct it, the mean squared error over the plane was computed for different bandwidths. We then took the one for which the error was lowest. To ease notation, we shall denote the corresponding estimator by  $\hat{f}_{b_{\text{opt}}}^{\text{Na}}$ , the nonadaptive estimator with same total search neighborhood as the final adaptive estimator by  $\hat{f}^{\text{Na}}$ . The estimator from our procedure will then be denoted by  $\hat{f}_{k_{\max}}^{\text{Ad}}$ . Figure 5.3 (a) provides box plots of the squared error over the time-frequency plane of these estimator with respect to the true spectral variates, i.e.,  $(\hat{f}(\cdot, \cdot) - f_{\text{true}}(\cdot, \cdot))^2$  for  $\hat{f} = \hat{f}_{b_{\text{opt}}}^{\text{Na}}$ ,  $\hat{f} = \hat{f}_{k_{\max}}^{\text{Ad}}$  and  $\hat{f} = \hat{f}^{\text{Na}}$ . It is clear that our method does much better, except in the extrema. This is intuitive, since the nonadaptive estimator will smooth out extremes such as a break while our method will detect the break but might be slightly off in terms of location. To illustrate, figure 5.3 (b) provides the frequency average of  $\hat{f}_{b_{\text{opt}}}^{\text{Na}}$  (red),  $\hat{f}_{k_{\max}}^{\text{Ad}}$  (blue) and the true spectrum  $f_{\text{true}}$  (green). It is clear that we are really close to detecting the break but that we are a few data-points off.

## 5.2. Locally stationary series

In the second example, we consider a time-varying moving average process of order 2 given by

$$X_{t,T} = \cos\left(2\pi \frac{t}{T}\right) Z_t - \left(\frac{t}{T}\right)^2 Z_{t-1}, \quad Z_t \stackrel{\text{iid}}{\sim} \mathcal{N}(0, 1). \quad (5.3)$$

The time-varying spectral density of this process, given by

$$f(u, \lambda) = \frac{1}{2\pi} (\cos(2\pi u)^2 - 2u^2 \cos(2\pi u) \cos(\lambda) + u^4), \quad (5.4)$$

is depicted in Figure 5.4 (a). The spectrum exhibits a peak in the middle of the time-frequency plane with smooth hill-sides in frequency direction and steeper ones in time direction. The pre-periodogram and the estimated plane after the adaptive iteration are given in 5.4 (b) and 5.4 (c). The iterations are stopped after  $k_{\max} = 7$

and the corresponding final estimated spectrum  $\hat{f}_{k_{\max}}^{\text{Ad}}$  is given in Figure 5.4 (d). The penalty and adaptive kernel for the midpoint  $(u, \lambda) = (0.5, 0)$  are provided in Figure 5.5. Barely any penalization is visible which is in line with the smoothness properties of the underlying process. However, we also observe (Fig. 5.4 (e)) that the nonadaptive estimated spectrum  $\hat{f}^{\text{Na}}$  with comparable bandwidths clearly out smooths the curvature. A comparison of the squared errors in Figure 5.6 (a) shows our adaptive procedure outperforms the optimal nonadaptive estimated spectrum. Although less convincing than in the previous case, this is still interesting as the original process is close to stationary. Over-smoothing by a global bandwidth will therefore not pose the same problem as it does for processes that exhibit a higher degree of nonstationarity. Figure 5.6 (b) gives the average over frequencies and demonstrates our method captures the curvature better than the nonadaptive estimates with optimal global bandwidths.

### 5.3. Structural break in locally stationary series

We now combine the above two processes. More precisely, we consider a white noise process that at  $t_0 = 410$  turns into an moving average process with similar dynamics as in the previous example but shifted in time. Thus we have

$$X_{t,T} = \sigma Z_t 1_{\{t \leq t_0\}} + \left[ \cos\left(2\pi\left(\frac{t}{T} - \frac{1}{5}\right)\right) Z_t - \left(\frac{t}{T} - \frac{1}{5}\right)^2 Z_{t-1} \right] 1_{\{t > t_0\}} \quad (5.5)$$

with  $Z_t \stackrel{\text{iid}}{\sim} \mathcal{N}(0, 1)$ . The corresponding time-varying spectral density is given by

$$f(u, \lambda) = \frac{\sigma^2}{2\pi} 1_{\{u \leq t_0/T\}} + g\left(u - \frac{1}{5}, \lambda\right) 1_{\{u > t_0/T\}}, \quad (5.6)$$

where  $g(u, \lambda)$  is as in (5.4). These type of spectra can for example occur when a signal is constant for a while and then receives a stimulus. This time-varying spectrum is interesting as the peak and the break are both close in distance as well as in level and hence are difficult to resolve. The estimation results are depicted in Figures 5.7 to 5.9. The algorithm is also in this case stopped after  $k = 7$  iterations. For visual comparison, we additionally included (Fig. 5.7 (d)) the nonadaptive estimated spectrum  $\hat{f}^{\text{Na}}$ . It can be seen to suffer clearly from over-smoothing. Figure 5.8 (a)–(b) show strong penalization in time direction and close to none in frequency direction for the midpoint, which lies in the valley. This is in accordance with the different slopes in the two directions. Compared to the previous case, the better performance compared to the optimal global bandwidth proxy is much more pronounced (Fig. 5.7 (a)). In particular, it can be seen in 5.9 (d), that the adaptive estimated plane again better captures the features of the true spectrum.

To see whether our conclusions depend on the variance level of the white noise before the structural break, we also consider the case where  $\sigma^2 = 3$ . The corresponding plots are in Figures 5.10 to 5.12. The penalty kernel of the midpoint now shows a quicker cut-off for the break point than in the lower variance case (Fig. 5.8 (a)–(b)). The adaptive kernel turns out as expected and gives full weight in frequency direction while it stops smoothing in time direction for areas outside the valley (Fig. 5.11 (a)–(b)). In terms of errors, also here our data-adaptive procedure shows a clear improvement compared to the optimal global bandwidth proxy.

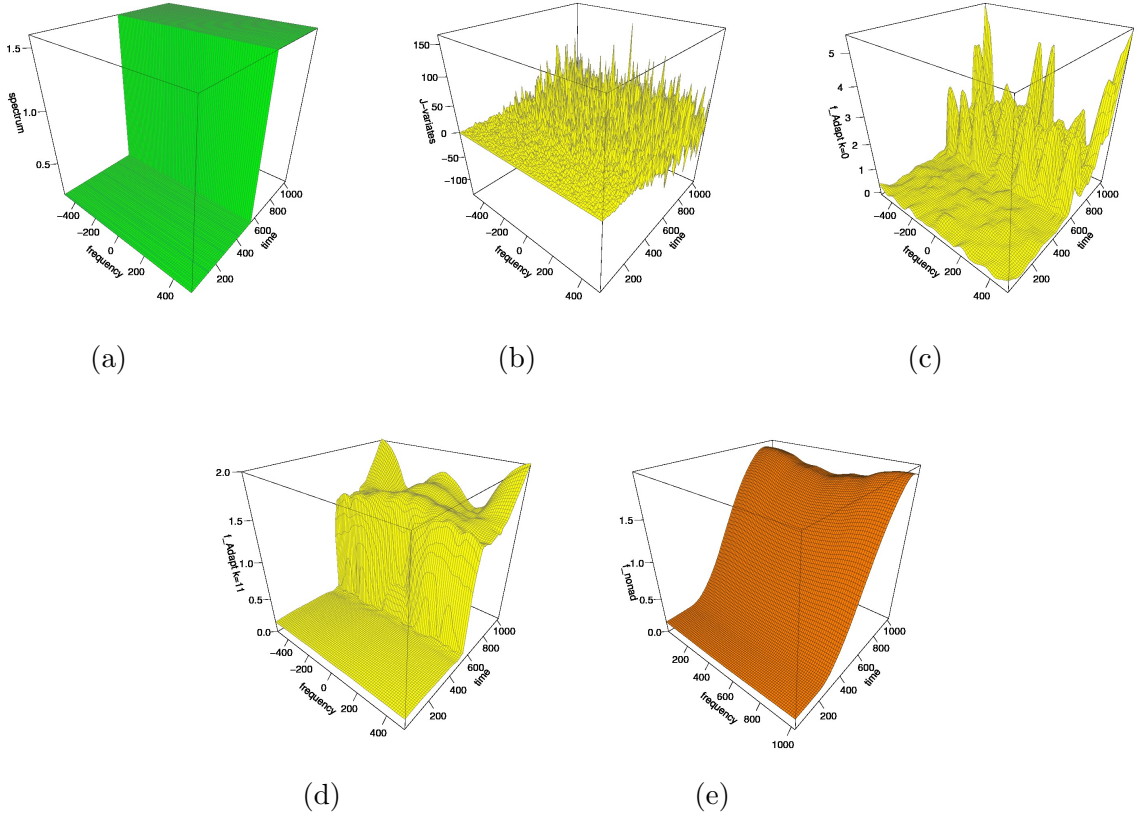


FIGURE 5.1. Example (5.1): true spectrum (a); pre-periodogram (b); adaptive estimated spectrum for  $k = 0$  (c) and for  $k_{\max} = 11$  (d); non-adaptive estimated spectrum  $\hat{f}^{\text{Na}}$  (e).

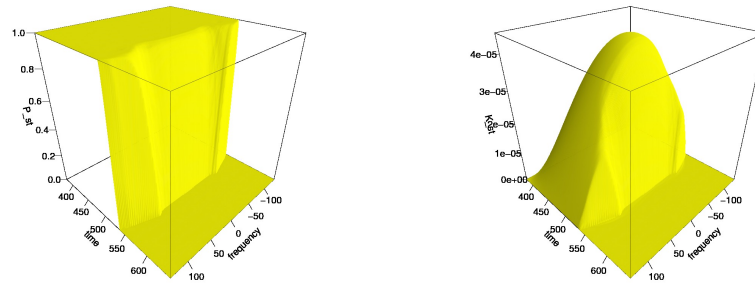


FIGURE 5.2. Penalty kernel (left) and adaptive kernel (right)  $\hat{f}_{k_{\max}}^{\text{Ad}}$  for  $k_{\max} = 11$  at  $(u, \lambda) = (0.5, 0)$ .

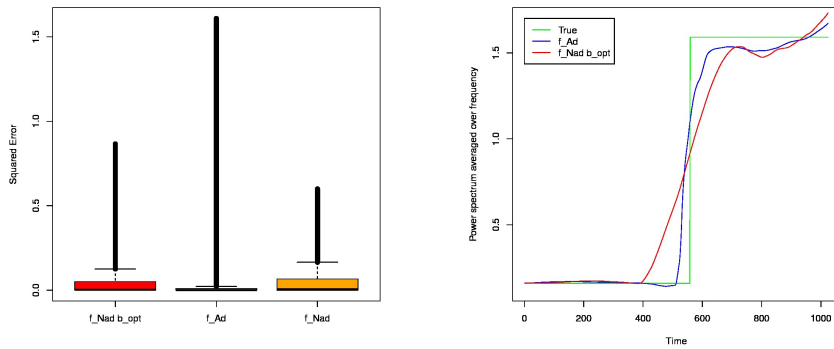


FIGURE 5.3. Squared error (left) and frequency average (right) of  $\hat{f}_{b_{\text{opt}}}^{\text{Na}}$ ,  $\hat{f}_{k_{\max}}^{\text{Ad}}$  and  $\hat{f}^{\text{Na}}$ , respectively.



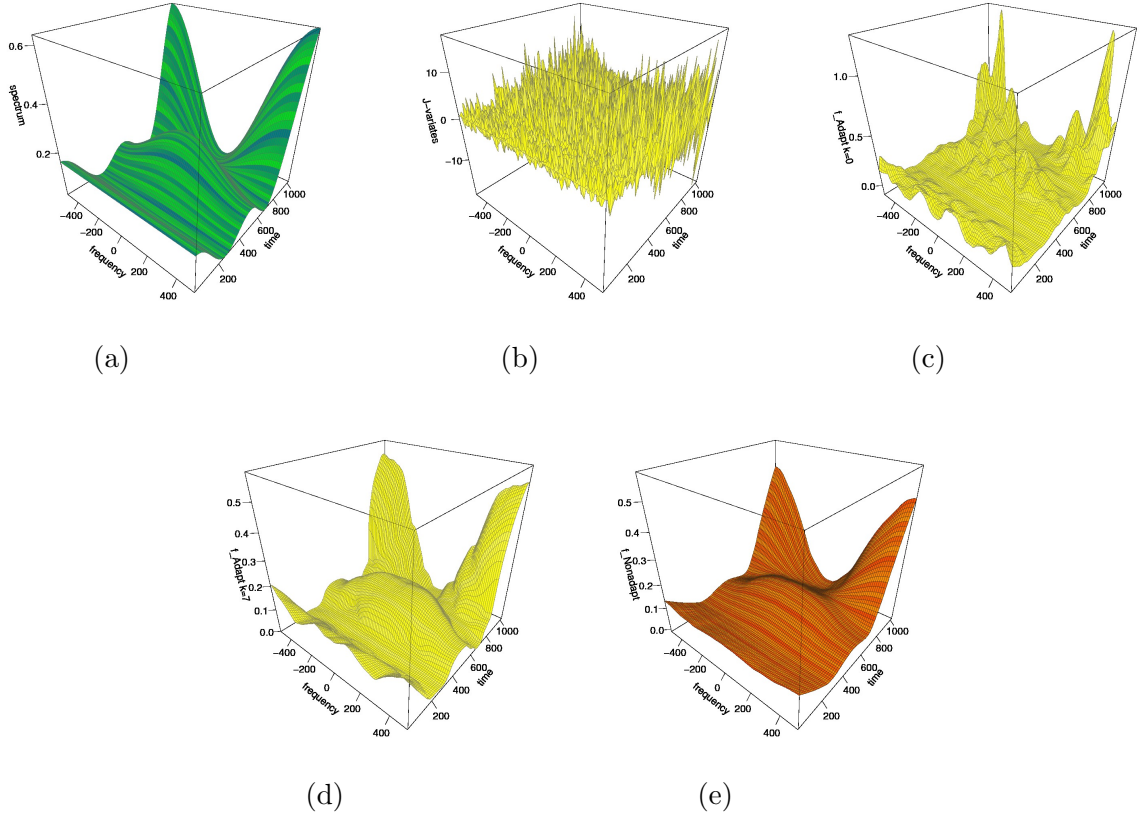


FIGURE 5.4. Example in (5.2): true spectrum (a); pre-periodogram (b); adaptive estimated spectrum for  $k = 0$  (c) and for  $k_{\max} = 7$  (d); nonadaptive estimated spectrum  $\hat{f}^{\text{Na}}$  (e).

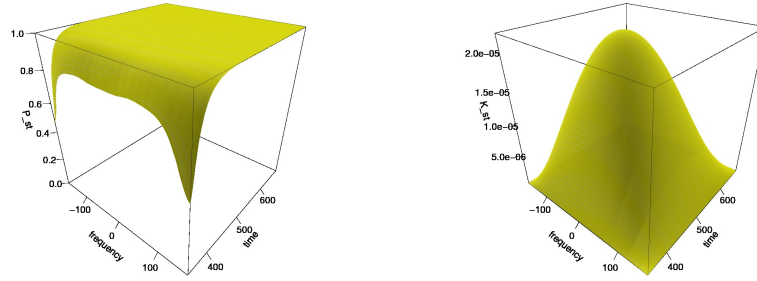


FIGURE 5.5. Penalty kernel (left) and adaptive kernel (right)  $\hat{f}_{k_{\max}}^{\text{Ad}}$  for  $k_{\max} = 7$  at  $(u, \lambda) = (0.5, 0)$ .

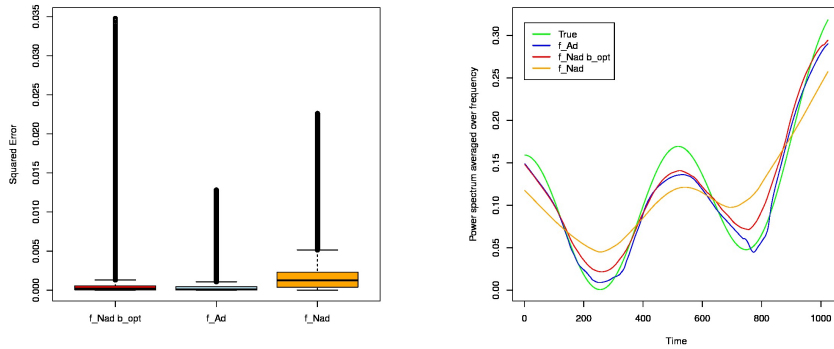


FIGURE 5.6. Squared error (left) and frequency average (right) of  $\hat{f}_{b_{\text{opt}}}^{\text{Na}}$ ,  $\hat{f}_{k_{\max}}^{\text{Ad}}$  and  $\hat{f}^{\text{Na}}$ , respectively.

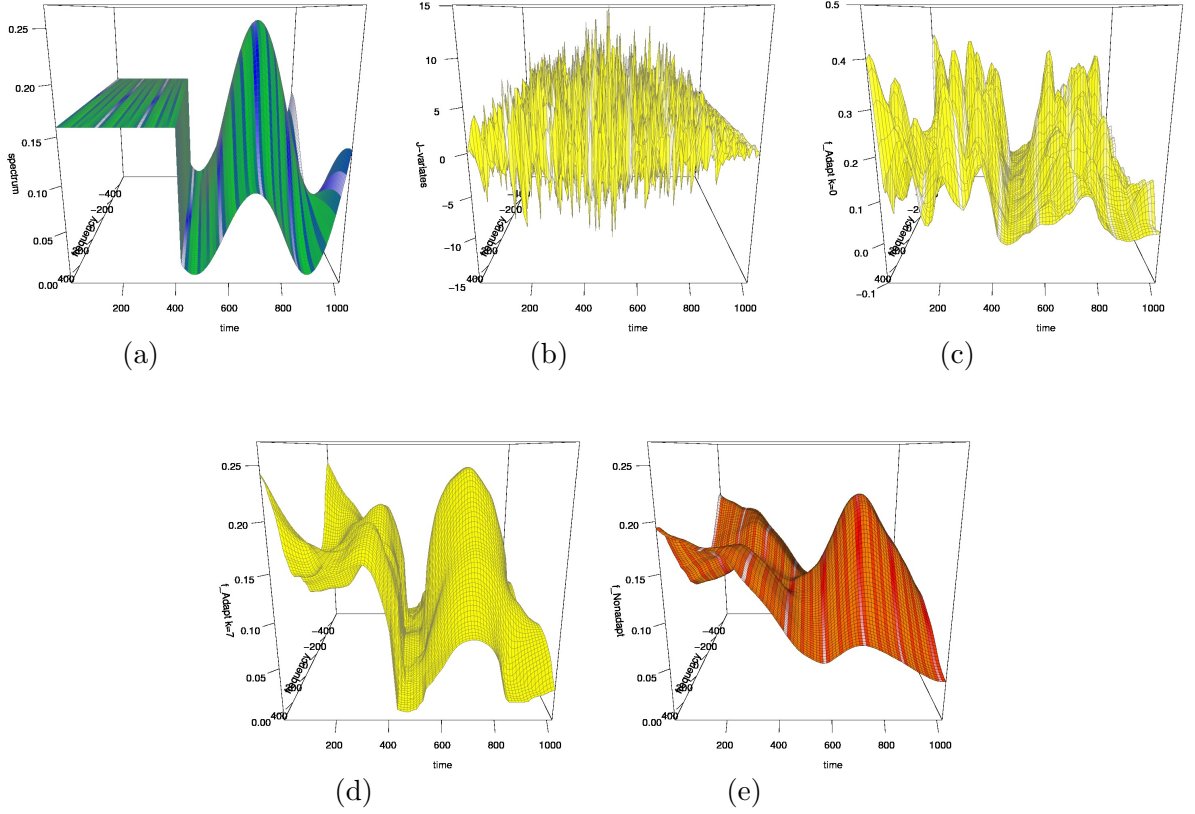


FIGURE 5.7. Example in (5.3) with  $\sigma = 1$ : true spectrum (a); pre-periodogram (b); adaptive estimated spectrum for  $k = 0$  (c) and for  $k_{\max} = 7$  (d); nonadaptive estimated spectrum  $\hat{f}^{\text{Na}}$  (e).

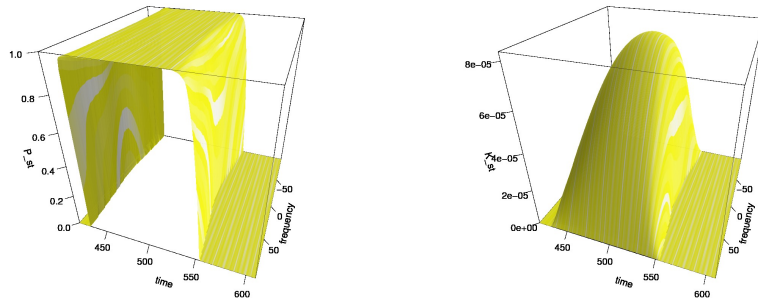


FIGURE 5.8. Penalty kernel (left) and adaptive kernel (right)  $\hat{f}_{k_{\max}}^{\text{Ad}}$  for  $k_{\max} = 7$  at  $(u, \lambda) = (0.5, 0)$ .

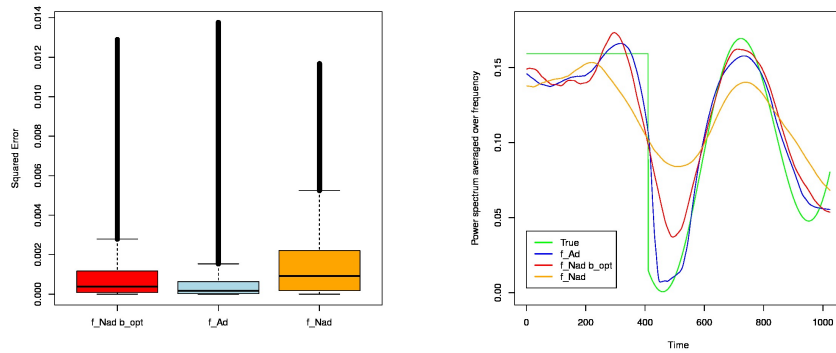


FIGURE 5.9. Squared error (left) and frequency average (right) of  $\hat{f}_{b_{\text{opt}}}^{\text{Na}}$ ,  $\hat{f}_{k_{\max}}^{\text{Ad}}$  and  $\hat{f}^{\text{Na}}$ , respectively.

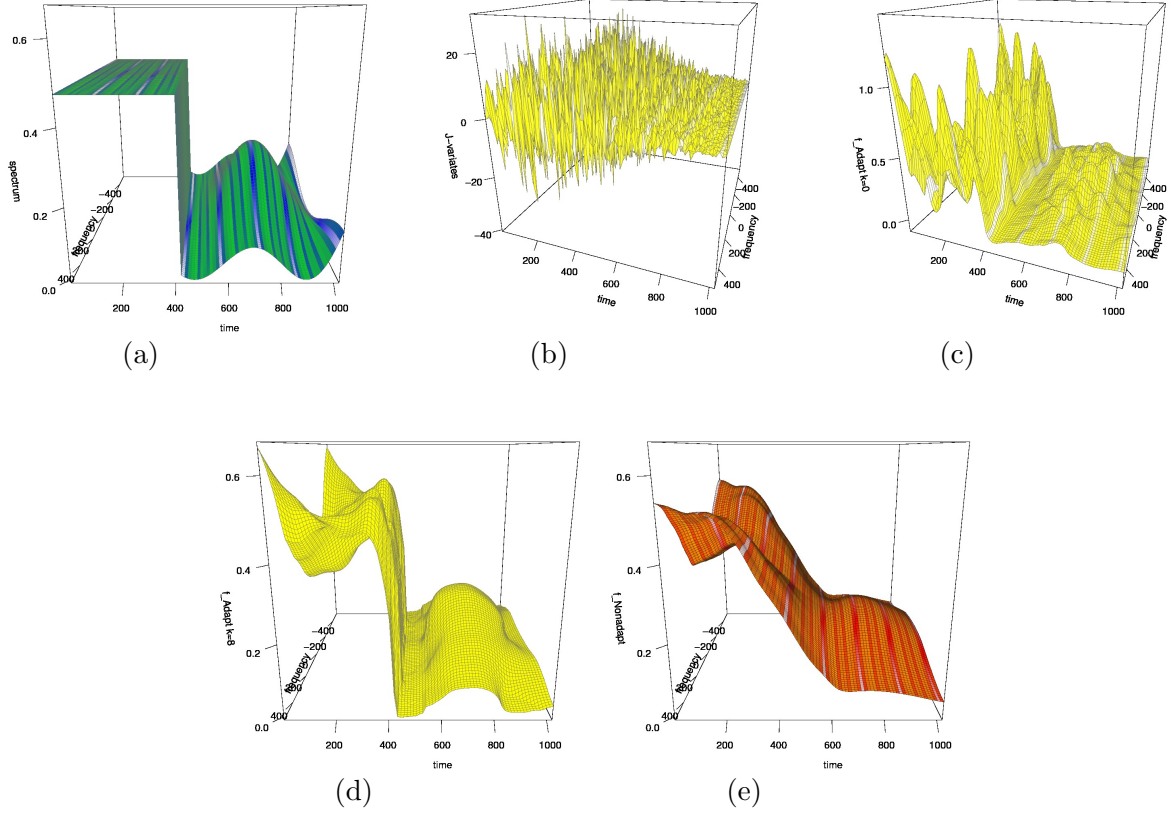


FIGURE 5.10. Example in (5.3) with  $\sigma = 3$ : true spectrum (a); pre-periodogram (b); adaptive estimated spectrum for  $k = 0$  (c) and for  $k_{\max} = 8$  (d); nonadaptive estimated spectrum  $\hat{f}^{\text{Na}}$  (e).

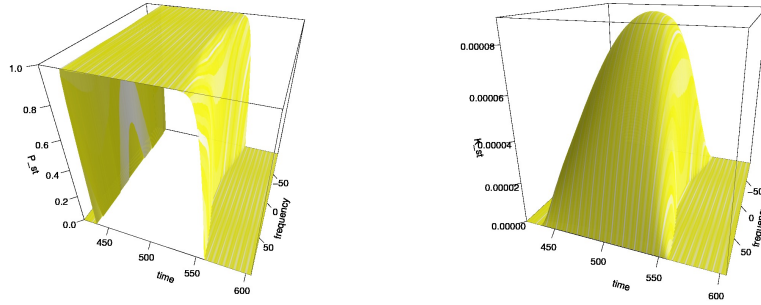


FIGURE 5.11. Penalty kernel (left) and adaptive kernel (right)  $\hat{f}_{k_{\max}}^{\text{Ad}}$  for  $k_{\max} = 8$  at  $(u, \lambda) = (0.5, 0)$ .

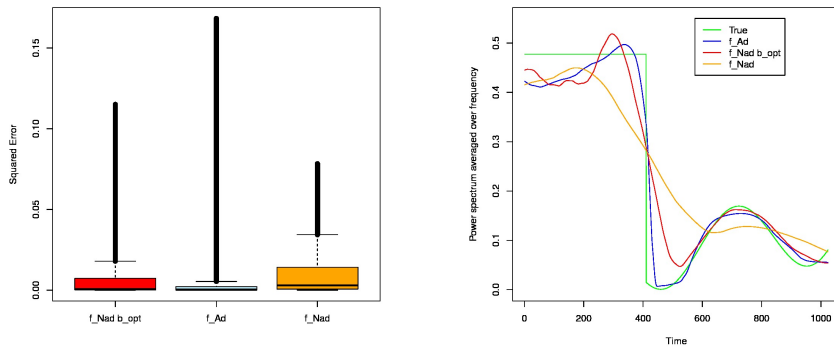


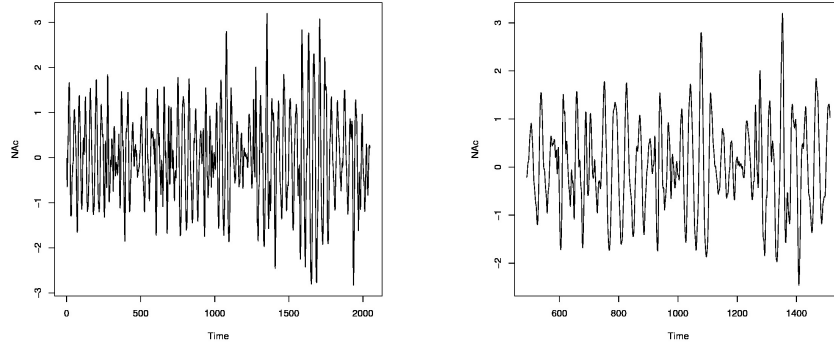
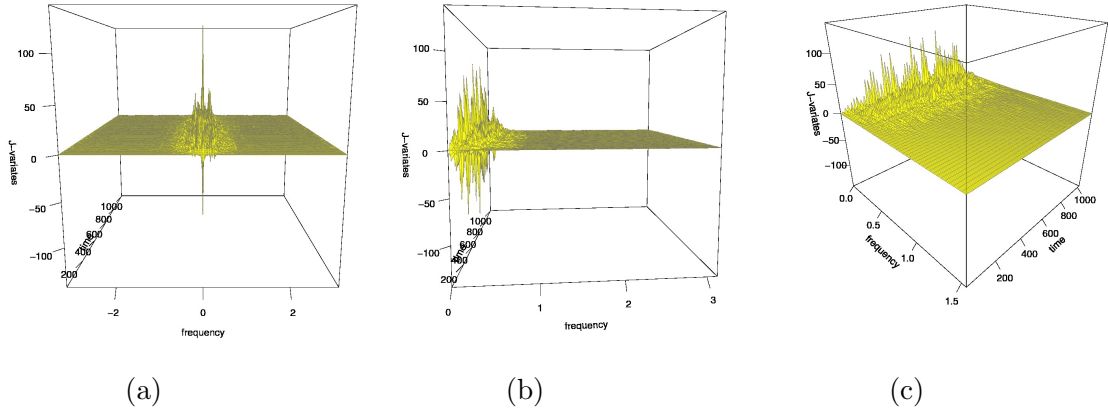
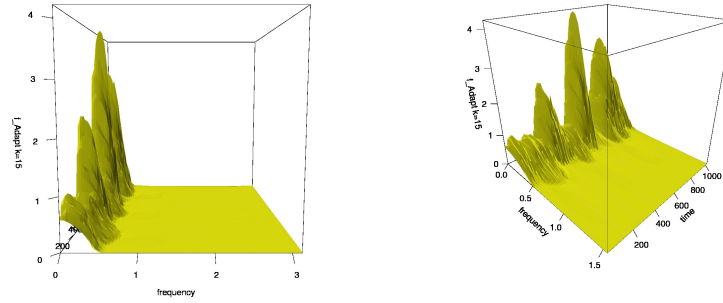
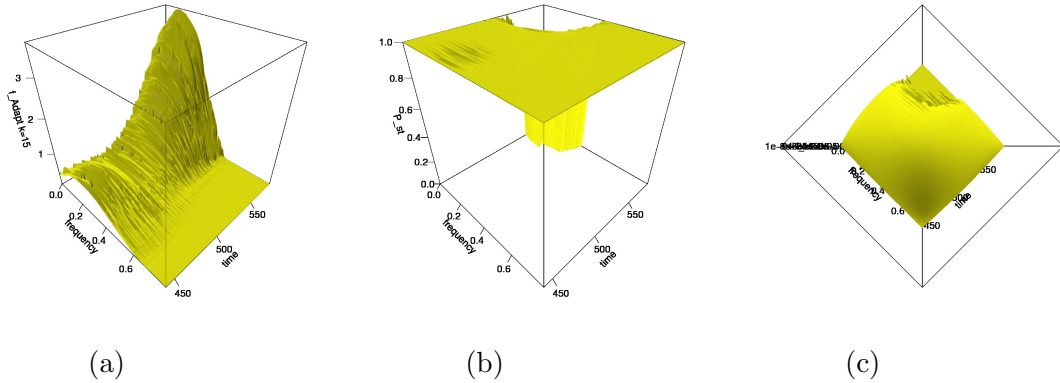
FIGURE 5.12. Squared error (left) and frequency average (right) of  $\hat{f}_{b_{\text{opt}}}^{\text{Na}}$ ,  $\hat{f}_{b_{\text{opt}}}^{\text{Ad}}$  and  $\hat{f}_{b_{\text{opt}}}^{\text{Na}}$ , respectively.

## 6. APPLICATION TO LOCAL FIELD POTENTIALS

As an application of our method, we consider local field potential (LFP) recordings of the nucleus accumbens of a male macaque monkey during an associative learning experiment. The experiment was conducted at the Neurosurgery Department at the Massachusetts General Hospital. During each trial, the monkey was shown four pictures and then had to select one of four doors. If the monkey made the correct association between picture and door he would receive a reward. In total, the learning experiment consisted of 675 trials. During the experiment, local field potentials were recorded of the nucleus accumbens and the hippocampus. In Fiecas and Ombao (2016), the nature of the dynamic interactions between these were investigated. There is clear evidence of nonstationary behavior within the trials, something that has also been observed in other types of brain data. It is therefore interesting to see if our method can capture this nonstationary behavior.

In Fig 6.1 we have the data of one of the trials. For our purposes, we consider the stretch of data  $t \in [490 : 1513]$  as this shows interesting behavior in time direction. A first inspection of the pre-periodogram (Fig 6.2(a)-(b)) indicates most of the neuronal activity is centered really close to frequency zero. In order to resolve the narrow peak(s), a small bandwidth is required in frequency direction. In particular, it is well-known from the stationary setting the width of the main lobe from the kernel function should be no larger and preferably half the size than the bandwidth of the narrowest peak in the spectrum. However, if it is set too conservative the erratic behavior of the pre-periodogram will be carried over to the estimates. Moreover, there is also clear evidence of nonstationary behavior in time direction (Fig 6.2(c)). Given the length of data, any starting bandwidths for which Assumption 3.7(ii) holds might out-smooth most of this behavior. In order to still capture the activity and deal with possible more volatile behavior, we set  $b_{t,T}^{(0)} = b_{f,T}^{(0)} = 0.05$ ,  $\gamma_t = \gamma_f = 1.1$  and  $b_T^{(0)*} = b_T^{(0)**} = b_{f,T}^{(0)}/2$ . Additionally,  $c = 2\chi_{1,0.99}^2$  and  $c_{mem} = 2\chi_{1,0.5}^2$  to take into account there will be more variation due to the small starting bandwidths. The rest of the parameters are the same as in section 5.

The estimated spectrum is given in Figure 6.3. Despite the fact that the stretch of data might not give enough resolution to resolve the exact peak location, it is clearly estimated away from zero. We observe some definite changes in both width and location of the peak over time. Figure 6.4 shows the estimated spectrum locally around the point  $(u, \lambda) = (0.5, 0.362)$ . We see rough patches here and there due to the low starting bandwidths but overall good adjustment of the penalty- and final kernel to the local peak. Although some effect of the cross-interference terms are visible in the final estimate, the overall estimated time-frequency plane appears to capture local structures reasonably well. This is promising given that the assumption of the underlying penalty statistic are not completely satisfied.

FIGURE 6.1. Time series Nac trial (left) and sub-stretch (right) over  $[490, 1513]$ .FIGURE 6.2. Pre-periodogram over  $(-\pi, \pi]$  (a) and over  $[0, \pi]$  for different angles (b)-(c).FIGURE 6.3. estimated spectrum  $k_{\max} = 15$  over  $[0, \pi]$  (left) and over  $[0, \pi/2]$  for different angles (right).FIGURE 6.4. estimated spectrum  $k_{\max} = 15$  around point  $(u, \lambda) = (0.5, 0.362)$  (a) with penalty kernel (b) and adaptive kernel (c), respectively.

## 7. CONCLUSION

In this paper, we introduced an adaptive kernel smoothing method for time-varying spectral densities. The method conceptually is based on the propagation-separation algorithm by Polzehl and Spokoiny (2006) but differs from it on essential points.

Firstly, although the algorithm by Polzehl and Spokoiny allows some smoothness, it is particularly designed to model piecewise constant functions. It will separate regions for which homogeneity is violated in a very strict manner. As an implication, such a method will favor identifying a steep hill-side as a structural break rather than a smooth transition. In contrast, the spectral density of a time series—stationary or non-stationary—is rarely piecewise constant over frequencies. Moreover, capturing the valleys and hill-sides of peaks in the spectrum form a particular difficulty that are of a very different nature than what can be found in pure time-domain analysis. Appropriately dealing with smoothly changing spectra requires that transitions from lower levels of energy to higher levels of energy are not being identified as a structural break. The method discussed in this paper is tailored to take this into account. Our way of penalizing, by means of the penalty kernel, is such that we allow for a smoother transition between adjacent points so that too quick separation is prevented.

Secondly, the original propagation-separation method relies on a regularity condition that follows from the underlying assumption of an exponential family. Consequently, the sample should give more or less equal information for different local parameter values. This assumption will often be violated for processes of interest in this paper since peaks and curvature are the rule rather than the exception. Consequently, the difference between optimal bandwidths over the plane could be substantial. Despite the essence of the problem being essentially the same, namely finding the optimal region adaptively for estimation, our underlying assumptions and framework are thus quite different.

Admittedly, our method has its limitations. In particular, even though the extension to multivariate spectra is direct, the running time can become quite long for the series that are of interest to us ( $T > 600$ ). This is a drawback but can be solved by running the algorithm on the graphics processing unit. The other issue has to do with identification. In a way we run into the classical problem of trying to obtain both momentum and position and as noted in section 3.2, we cannot get them perfect at the same time. The balance that we need between optimal bandwidths and reliable updates requires that extremes should be over smoothed to some extent. However, the method allows for a high level of flexibility between final bandwidths for different points and the level of over-smoothing is much less than when a global bandwidth for all local variates is imposed. Empirical results show that in case of locally stationary processes with or without break, we obtain much lower errors. In particular, our method adjusts very well to the presence of a break in smooth changing spectra. The method is directly applicable to data and takes into account data features as presented to the researcher and does not rely too heavily on asymptotical results yet still obeys to its framework. Furthermore, it is robust under a variety of processes without fine-tuning of the parameters. It would be worth looking into the theoretical properties in more detail, possibly allowing optimizing parameter specification. Additionally, it is of general interest to

investigate a method that optimally reduces the effect of cross-interference terms of the underlying pre-periodogram. This is left for future research.

## REFERENCES

- Bartlett, M. (1950). Periodogram analysis and continuous spectra. *Biometrika* **37**, 1–16.
- Becker, S. and Mathé, P. (2013). A different perspective on the propagation-separation approach. *Electronic Journal of statistics* **7**, 2702–2736.
- Brillinger, D. (1981). *Time Series: Data Analysis and Theory*. McGraw Hill, New York.
- Cooley, J. and Tukey, J. (1965). An algorithm for the machine calculation of complex fourier series. *Mathematics of Computation* **19**(90), 297–301.
- Cramér, H. (1942). On harmonic analysis in certain functional spaces. *Arkiv för Matematik, Astronomi och Fysik* **28B**, 1–7.
- Dahlhaus, R. (1996a). Asymptotic statistical inference for nonstationary processes with evolutionary spectra. in: Robinson, P.M., Rosenblatt, M. (Eds.), *Athens Conference on Applied Probability and Time Series Analysis*, vol. II. Springer-Verlag, New York.
- Dahlhaus, R. (1996b). On the kullback-leibler information divergence of locally stationary processes. *Stochastic Process and their Applications* **62**(1), 139–168.
- Dahlhaus, R. (2009). Local inference for locally stationary time series based on the empirical spectral measure. *Journal of Econometrics* **151**, 101–112.
- Dahlhaus, R. and Polonik, W. (2009). Empirical spectral processes for locally stationary time series. *Bernoulli* **15**, 1–39.
- Eichler, M., Motta, G. and von Sachs, R. (2011). Fitting dynamic factor models to non-stationary time series. *Journal of Econometrics* **163**(1), 51–70.
- Fiecas, M. and Ombao, H. (2016). Modeling the evolution of dynamic brain processes during an associative learning experiment. *Journal of the American Statistical Association* accepted manuscript.
- Grenander, U. and Rosenblatt, M. (1957). Statistical analysis of time series.
- Hallin, M. (1986). Nonstationary q-dependent processes and time-varying moving average models: invertibility properties and the forecasting problem. *Advances in Applied Probability* **32**, 170–210.
- Martin, W. Flandrin, P. (1985). Wigner-ville spectral analysis of nonstationary processes. *IEEE Trans. Signal Process* **33**, 1461–1470.
- Neumann, M. H. and von Sachs, R. (1997). Wavelet thresholding in anisotropic function classes and application to adaptive estimation of evolutionary spectra. *The Annals of Statistics* **25**(1), 38–76.
- Ombao, H., Raz, J., Von Sachs, R. and Malow, B. (2001). Automatic statistical analysis of bivariate nonstationary time series. *Journal of the American Statistical Association* **96**, 543–560.
- Polzehl, J. and Spokoiny, V. (2006). Propagation-separation approach for local likelihood estimation. *Probability Theory and Related Fields* **135**(3), 335–362.
- Preuß, P., Vetter, M. and Dette, H. (2011). Testing semiparametric hypotheses in locally stationary processes. Working paper, Ruhr-University Bochum.
- Priestley, M. B. (1965). Evolutionary spectra and non-stationary processes. *Journal of the Royal Statistical Society. Series B (Methodological)* **27**(2), 204–237.
- Sergides, M. and Paparoditis, E. (2009). Frequency domain tests of semiparametric hypotheses for locally stationary processes. *Scandinavian Journal of Statistics* **36**, 800–821.
- Subba Rao, T. (1970). The fitting of non-stationary time series models with time-dependent parameters. *Journal of the Royal Statistical Society. Series B (Methodological)* **32**, 312–322.